inorganics

MDPI

Review

From Porphyrinic MOFs and COFs to Hybrid Architectures: Design Principles for Photocatalytic H_2 Evolution

Maria-Chrysanthi Kafentzi, Grigorios Papageorgiou and Kalliopi Ladomenou *

Hephaestus Laboratory, School of Chemistry, Faculty of Science, Democritus University of Thrace, Kavala University Campus, St. Lucas, 65404 Kavala, Greece
* Correspondence: kladomenou@chem.duth.gr

Abstract

Solar-driven hydrogen production via photocatalytic water splitting represents a promising route toward sustainable and low-carbon energy systems. Among emerging photocatalysts, porphyrin-based framework materials, specifically porphyrinic metal–organic frameworks (PMOFs) and porphyrinic covalent organic frameworks (PCOFs), have attracted increasing attention owing to their strong visible-light absorption, tunable electronic structures, permanent porosity, and well-defined catalytic architectures. In these systems, porphyrins function as versatile photosensitizers whose photophysical properties can be precisely tailored through metalation, peripheral functionalization, and integration into ordered frameworks. This review provides a comprehensive, design-oriented overview of recent advances in PMOFs, PCOFs, and hybrid porphyrinic architectures for photocatalytic H_2 evolution. We discuss key structure–activity relationships governing light harvesting, charge separation, and hydrogen evolution kinetics, with particular emphasis on the roles of porphyrin metal centers, secondary building units, linker functionalization, framework morphology, and cocatalyst integration. Furthermore, we highlight how heterojunction engineering through coupling porphyrinic frameworks with inorganic semiconductors, metal sulfides, or single-atom catalytic sites can overcome intrinsic limitations related to charge recombination and limited spectral response. Current challenges, including long-term stability, reliance on noble metals, and scalability, are critically assessed. Finally, future perspectives are outlined, emphasizing rational molecular design, earth-abundant catalytic motifs, advanced hybrid architectures, and data-driven approaches as key directions for translating porphyrinic frameworks into practical photocatalytic hydrogen-generation technologies.

Keywords: MOFs; COFs; porphyrins; hybrids; photocatalysts; photosensitizers; hydrogen evolution

Check for updates

Academic Editor: Francis Verpoort

Received: 30 December 2025
Revised: 21 January 2026
Accepted: 21 January 2026
Published: 23 January 2026

Copyright: © 2026 by the authors. Licensee MDPI, Basel, Switzerland. This article is an open access article distributed under the terms and conditions of the Creative Commons Attribution (CC BY) license.

1. Introduction

1.1. Global Need for Sustainable Hydrogen Production

Hydrogen (H_2) is increasingly recognized as a strategic energy carrier for deep decarbonization, owing to its high gravimetric energy density (120–142 $MJ \cdot kg^{-1}$) and its versatility as a chemical feedstock, transportation fuel, and medium for long-duration energy storage. According to the International Energy Agency Global Hydrogen Review 2023 [1], global hydrogen demand reached approximately 95 million metric tons (Mt) in 2022 and increased to around 97 Mt in 2023, with consumption largely concentrated in the refining and chemical sectors. Under most net-zero scenarios, this demand is projected to grow substantially in the coming decades [1,2]. Despite its potential, current hydrogen

production remains overwhelmingly carbon-intensive. The vast majority of H_2 is generated from fossil resources via steam methane reforming and coal gasification, processes that collectively emit approximately 0.9×10^9 t CO_2 annually. These emissions represent a significant contribution to global greenhouse-gas output and pose a major obstacle to achieving climate-neutral energy systems [2]. Consequently, the rapid development of low- and zero-carbon hydrogen production routes is an urgent priority. Solar energy, which is abundant, renewable, and globally accessible, offers a compelling pathway toward sustainable hydrogen generation. Solar-driven hydrogen production methods, including photoelectrochemical and photocatalytic water splitting, have attracted increasing attention because they enable direct conversion of sunlight into chemical fuel while minimizing upstream emissions [3,4]. In addition to environmental considerations, economic and resource constraints further motivate this transition. Declining discovery rates of new petroleum reserves, combined with steadily rising global energy demand, raise serious concerns regarding the long-term sustainability of fossil-fuel-dependent economies [5]. However, scaling low-carbon hydrogen production to meet projected future demand presents substantial system-level challenges. Full replacement of current hydrogen production with electrolytic ("green") hydrogen would require enormous additional electricity supplies. Using typical electrolysis energy intensities (50–60 kWh·kg^{-1} H_2), production of hundreds of megatons of hydrogen annually would demand several petawatt-hours (PWh) of renewable electricity, necessitating massive expansion of both power-generation and electrolyzer infrastructure [2]. In parallel, reliance on freshwater resources for large-scale hydrogen production may exacerbate global water scarcity. As a result, photoinduced seawater splitting has emerged as a promising alternative, offering a route to sustainable hydrogen generation while reducing freshwater consumption [6].

Taken together, these environmental, economic, and resource considerations underscore the urgent need to accelerate research into diversified, scalable, and low-carbon hydrogen production pathways. In this context, solar-driven water splitting approaches that bypass the electrical grid and enable decentralized hydrogen generation are particularly attractive, placing renewed emphasis on the development of efficient and robust photocatalysts.

1.2. Photocatalytic H_2 Evolution: Principles and Current Challenges

Photocatalytic water splitting involves two coupled half-reactions: the hydrogen evolution reaction (HER) and the oxygen evolution reaction (OER). As illustrated in Figure 1, the overall process proceeds through three fundamental steps. First, upon irradiation with ultraviolet (UV), visible, or near-infrared (NIR) light, the photocatalyst absorbs photons with energies equal to or exceeding its band gap. In organic semiconductors, this band gap corresponds to the energy difference between the highest occupied molecular orbital (HOMO) and the lowest unoccupied molecular orbital (LUMO), whereas in inorganic semiconductors it is defined by the separation between the valence band (VB) and conduction band (CB) [7]. Photon absorption promotes electrons from the HOMO (or VB) to the LUMO (or CB), generating photogenerated electrons and holes [8].

Subsequently, these charge carriers migrate to the catalyst surface, where electrons reduce protons to produce H_2, while holes oxidize water to generate O_2. However, during migration, a significant fraction of electron–hole pairs recombine nonradiatively, resulting in substantial energy losses. Only charge carriers that successfully reach catalytically active surface sites contribute to the desired redox reactions, making charge separation and transport critical determinants of photocatalytic efficiency.

Photocatalytic water splitting is thermodynamically uphill ($\Delta G > 0$). For efficient operation, the CB edge of the photocatalyst must be more negative than the H^+/H_2 reduction potential (0.0 V vs. NHE at pH 0), while the VB edge must be more positive than the

O_2/H_2O oxidation potential (1.23 V vs. NHE at pH 0) [9]. Consequently, an ideal photocatalyst typically possesses a band gap in the range 1.23 eV < E_g < 3.0 eV, corresponding to light absorption between approximately 400 and 1000 nm [10].

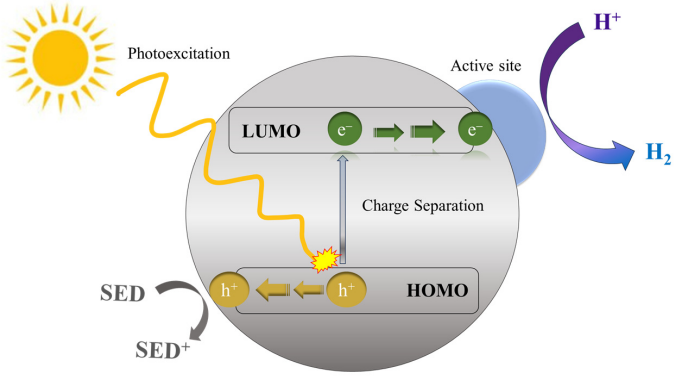


Figure 1. Mechanism involved for photocatalytic hydrogen evolution. SED: sacrificial electron donor; SED^+: sacrificial electron donor (oxidized species).

To enhance photocatalytic activity and suppress recombination, several strategies have been developed, including loading cocatalysts to facilitate charge extraction and reduce overpotentials, employing sacrificial electron donors to scavenge photogenerated holes, and constructing heterostructures with complementary band alignments [11]. In heterostructured systems, photogenerated electrons and holes can be spatially separated across different components, significantly improving charge-carrier lifetimes and utilization efficiency [12].

Despite considerable progress, practical photocatalytic hydrogen production remains limited by several persistent challenges [13–24]. These include insufficient visible-light absorption in many stable materials, ultrafast charge recombination at defects or trap states, continued reliance on noble-metal cocatalysts to achieve high activity, and low long-term stability under aqueous reaction conditions. Overcoming these barriers requires next-generation photocatalytic architectures that combine long-lived excited states, atomically efficient catalytic sites, broad and tunable light-harvesting capabilities, and engineered pathways for rapid charge extraction [3,10].

1.3. Advantages of Porphyrinic Frameworks (PMOFs and PCOFs) for Solar Hydrogen Generation

Porphyrins are macrocyclic heteroaromatic molecules derived from porphin (Figure 2) and are distinguished by intense Soret and Q absorption bands, rich redox chemistry, and exceptional structural versatility [25].

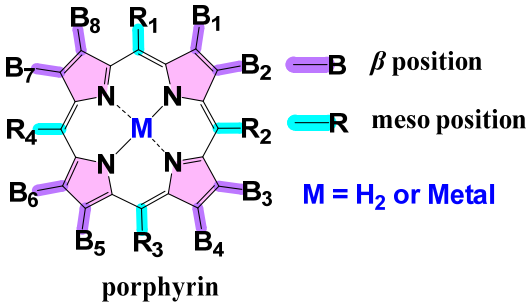


Figure 2. Schematic representation of the porphyrin macrocycle, where M denotes H_2 or a coordinated metal ion, and R_1–R_4 and B_1–B_8 correspond to substituents at the meso and β positions, respectively.

Their photophysical properties can be precisely tuned through metalation of the central cavity and functionalization at the meso or β positions (Figure 2), enabling control over

excited-state lifetimes, redox potentials, and catalytic behavior [26]. These attributes make porphyrins highly attractive chromophores for solar energy conversion.

Porphyrins impart a unique combination of molecular-level tunability, long-range structural order, and permanent porosity. This integration offers an effective strategy for addressing the interconnected challenges of light harvesting, charge separation, and catalytic activity in photocatalytic systems [26].

Porphyrinic frameworks provide several synergistic advantages for photocatalytic hydrogen evolution. First, their photophysical properties can be systematically engineered via porphyrin metalation and peripheral functionalization, enabling fine control over band-edge positions, excited-state dynamics, and redox thermodynamics. Second, the site-isolation and confinement effects inherent to framework architectures stabilize atomically dispersed catalytic centers and enable controlled nucleation of cocatalyst nanoparticles. Third, permanent porosity and interconnected channels facilitate efficient mass transport of protons, sacrificial agents, and reaction products. Finally, precise control over framework morphology and crystallinity shortens charge-transport distances and suppresses bulk recombination losses, thereby enhancing photocatalytic efficiency [26,27].

Furthermore, metal–organic frameworks (MOFs) are a class of crystalline porous nanomaterials consisting of metal nodes and organic ligands connected through coordination interactions [28]. Covalent organic frameworks (COFs) are a class of organic porous materials constructed from organic building blocks linked by covalent bonds resulting in an extended periodic structure [29]. When porphyrins are incorporated as organic linkers into MOFs or COFs, this results in the construction of porphyrinic MOFs (PMOFs) and porphyrinic COFs (PCOFs).

In this review, we adopt a design-oriented perspective to summarize recent advances in photocatalytic hydrogen production using PMOFs, PCOFs, and related hybrid architectures. We focus on key structural and compositional parameters including linker chemistry, metal incorporation strategies, framework topology, and interfacial engineering and discuss how these factors govern photophysical behavior, hydrogen evolution kinetics, and operational stability. Although several reviews have addressed porphyrin-based frameworks for H_2 evolution [7,9,26,30–32], the present manuscript specifically emphasizes developments from the past five years in PMOFs, PCOFs, and hybrid porphyrin-based architectures, establishing clear correlations between structural features and photocatalytic HER performance. To the best of our knowledge, no existing review provides a comprehensive and design-focused analysis of these interconnected aspects. By articulating rational design principles for high-performance porphyrinic frameworks, this review aims to guide future research toward scalable, durable, and efficient materials for solar hydrogen generation.

2. Porphyrinic Metal–Organic Frameworks (PMOFs) for H_2 Evolution

2.1. Structural Design Principles of PMOFs

The structural characteristics that control light absorption, charge separation, and accessibility of active sites play a decisive role in determining the photocatalytic performance of porphyrinic metal–organic frameworks (PMOFs). Among these factors, the nature of the porphyrin linker is particularly critical. Chemical modification of the porphyrin periphery (Figure 2) enables fine tuning of electron affinity and energy levels, facilitating the development of PMOFs with enhanced visible-light harvesting, improved charge separation, and more efficient charge transport [25]. In addition, the porphyrin core can coordinate a wide range of metal ions, allowing catalytically active sites to be incorporated directly into the framework backbone. Compared with free-base porphyrins, metalation of tetrakis(4-carboxyphenyl) porphyrin (TCPP)-type linkers with metals such as Zn, Co, or Ni alters the HOMO-LUMO gap and stabilizes long-lived excited states, leading to markedly

enhanced hydrogen evolution efficiencies [33]. Equally important is the choice of secondary building units (SBUs) [34]. Functionalization of porphyrinic carboxylates with metal–oxo clusters results in strong linker–node coupling and rigid framework architectures. Notably, many PMOFs operate through a ligand-to-metal charge-transfer (LMCT) mechanism, in which porphyrin linkers serve as the primary light-harvesting units while the metal nodes act as catalytic or electron-accepting sites. Upon photoexcitation, electrons generated on the porphyrin ligands are transferred to the metal nodes through π-conjugated pathways, effectively promoting charge-carrier separation and suppressing recombination [28]. Among the most widely employed SBUs for photocatalytic hydrogen evolution are zirconium- and titanium-based metal–oxo clusters, as well as paddle-wheel-type nodes ($M_2(COO)_4$). In addition to the framework composition, the morphology and spatial arrangement of porphyrin units critically influence photocatalytic activity. High crystallinity and mesoporosity enhance mass transport, while closely packed porphyrin arrays facilitate exciton migration and electronic communication. Nanoscale and ultrathin PMOF architecture consistently exhibit superior hydrogen evolution rates compared with their bulk counterparts. PMOF nanosheets are especially advantageous because they shorten charge-migration distances, minimize bulk recombination, and expose a higher density of accessible catalytic sites [26]. Further performance enhancements can be achieved through heterostructure engineering, in which PMOFs are coupled with inorganic semiconductors or decorated with cocatalysts such as Pt, Pd, or Ni. These hybrid interfaces create favorable band alignments, accelerate photogenerated electron extraction, and improve overall charge utilization. Indeed, representative PMOF-semiconductor composites have demonstrated significantly enhanced hydrogen evolution rates because of efficient interfacial charge separation at the heterojunctions [35]. Finally, structural robustness is a critical requirement for practical photocatalytic applications. Zr-based porphyrinic frameworks exhibit exceptional resistance to loss of crystallinity and photocatalytic activity under prolonged irradiation and aqueous reaction conditions, outperforming MOFs constructed from weaker metal–linker bonds. Consequently, stability considerations strongly influence both SBU selection and synthetic strategy [27]. Collectively, these considerations on porphyrin metalation, SBU selection, morphological control, interfacial engineering, and structural stability define a coherent design roadmap for constructing next-generation PMOFs optimized for efficient and durable photocatalytic hydrogen evolution.

2.2. Influence of Linker Functionalization and Functional Groups of PMOFs

PMOFs can be finely modulated in their photophysical and electronic properties by incorporating different functional groups onto the porphyrin linkers. Generally, electron-donating substituents (for example, $-NH_2$) increase the level of the ligand HOMO and usually reduce the band gap of the MOF, which enhances visible-light absorption and promotes charge excitation. In contrast, electron-withdrawing substituents (for example, $-NO_2$ and $-SO_3H$, halogen atoms) lower the level of the ligand LUMO and can deepen both frontier orbitals, shifting the band edges for better thermodynamic alignment with proton reduction. These electronic effects have direct consequences on charge separation: donors may enhance the excited-electron population and accelerate their injection into catalytic sites, whereas acceptors may prolong charge separation by providing internal charge-transfer pathways (donor–acceptor, D-A). Functionally, polar groups like $-SO_3H$ or additional -COOH moieties enhance MOF hydrophilicity and proton access to active sites [36]. Tetrakis(4-carboxyphenyl) porphyrin (TCPP), consisting of a porphyrin core bearing four benzoic acid substituents, is one of the most widely used porphyrinic ligands for constructing PMOFs, either as a free base or in one of its metalated forms to investigate HER activity. The presence of highly polar substituents (carboxylates) in meso positions of

TCPP, in combination with an ordered nanocrystalline architecture of the resulting PMOF, enables efficient separation of photogenerated charge carriers and therefore enhances the photocatalytic activity of TCPP-based MOFs. Furthermore, TCPP forms durable coordination bonds within MOFs, imparting excellent chemical and thermal stability. Such polar substituents can increase pore surface polarity, aid water adsorption and proton transport, and often enlarge surface area. Indeed, linker functionalization often increases MOF porosity and reduces the optical gap, thereby boosting overall photocatalytic activity [28]. For example, a D-A PMOF, designated TCPP-Zn-BTDO, was developed by coordinating TCPP as the electron-donor unit, with the electron acceptor dibenzothiophene-S,S-dioxide (BTDO), through Zn^{2+} linkages (Figure 3) [37]. The inclusion of the sulfone-containing BTDO fragment imparts a strong electron-withdrawing character, a planar conjugated structure, and favorable hydrophilicity, making it well suited for photocatalytic HER. This D-A architecture expands the spectral absorption range, creating more photogenerated carriers. At the same time, more efficient charge separation is enhanced that suppresses their recombination, resulting in boosting H_2-production performance, accounting for 1.48 $mmol \cdot g^{-1} \cdot h^{-1}$ (Entry 1, Table 1).

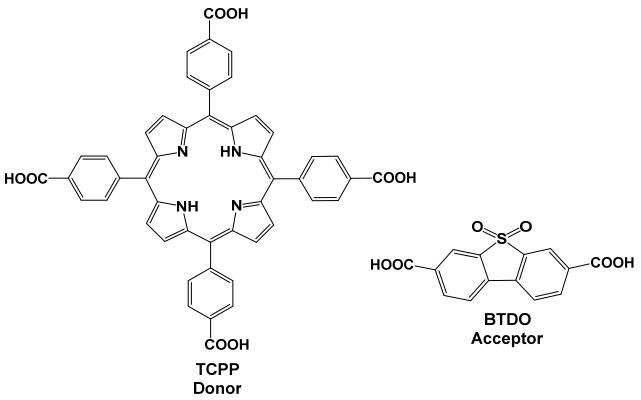


Figure 3. Schematic representation of TCPP and BTDO.

2.3. Impact of SBU of MOFs

The metal nodes in porphyrinic MOFs play a crucial role in imposing structural rigidity and long-range order on the porphyrin linkers, thereby stabilizing them within the framework, preventing undesirable aggregation or conformational distortion, and ultimately increasing the accessibility of catalytically active sites for photocatalytic reactions [28]. Metal-based secondary building units (SBUs), including metal ions and metal–oxo clusters, typically coordinate to the carboxylate groups of porphyrin ligands. Titanium ions commonly form TiO_6 octahedral clusters, while zirconium ions generate highly connected Zr_6 oxo-cluster nodes. Copper ions, in contrast, frequently form paddle-wheel-type $Cu_2(COO)_4$ SBUs through chelation with polycarboxylate ligands.

Among these systems, Zr-based PMOFs exhibit outstanding chemical and photochemical stability, as well as enhanced visible-light absorption when combined with porphyrinic linkers. These properties arise from the high oxidation state of Zr(IV) and the high connectivity of the Zr-oxo SBUs, which confer exceptional framework robustness [28]. Titanium-based metal–organic frameworks (Ti-MOFs) have also attracted considerable interest as photocatalysts due to their high surface areas, excellent thermal stability, and tunable electronic properties [38,39]. In Ti-MOFs, photosensitizing units and catalytic sites are spatially integrated within a microcrystalline porous architecture, which effectively suppresses electron-hole recombination. Also, their permanent porosity and accessible metal sites promote efficient mass transport of reactants and facilitate their interaction with active centers, further enhancing photocatalytic performance [40].

A representative example is the Ti-oxo cluster-based PMOF "TMF-Pt", reported by Feng et al., which was constructed via a thermolytic reaction between $TiCl_4$ and Pt (II)-metalated TCPP linkers, yielding a robust three-dimensional framework. Under visible-light irradiation, TMF-Pt exhibited an exceptionally high hydrogen evolution rate of 15.456 $mmol \cdot g^{-1} \cdot h^{-1}$ (Entry 2, Table 1), ranking among the highest reported PMOF-based photocatalysts. This remarkable activity was attributed to the efficient utilization of Pt(II) centers embedded within the porphyrin cores and the effective ligand-to-cluster charge transfer (LCCT) facilitated by the Ti-oxo nodes [41].

Additionally, Zr-based PMOFs showed excellent stability and extensive visible-light absorption performance after binding porphyrin due to the high valence state of Zr (IV) and the high connection number of SBU [28]. In one study, a Zr (IV)-based PMOF (PCN-221) composed of M(II)-TCPP linkers and Zr_8O_6 SBUs was investigated to elucidate the contribution of Zr clusters to catalytic activity. However, it has been revealed that PCN-221 consists of $Zr_6O_4(OH)_4$ clusters in four distinct orientations rather than Zr_8O_6 clusters [42]. Upon 24 h of irradiation, Zn-TCPP alone produced 0.600 $mmol \cdot g^{-1}$ of H_2, whereas the addition of approximately eight equivalents of the Zr-oxo cluster increased hydrogen production to 2.800 $mmol \cdot g^{-1}$ in homogeneous solution, comparable to the performance of solid PCN-221(Zn), which yielded 2.230 $mmol \cdot g^{-1}$. These results strongly support the hypothesis that Zr-oxo clusters function as catalytic centers that facilitate effective LCCT (Figure 4), a key factor governing photocatalytic efficiency [43].

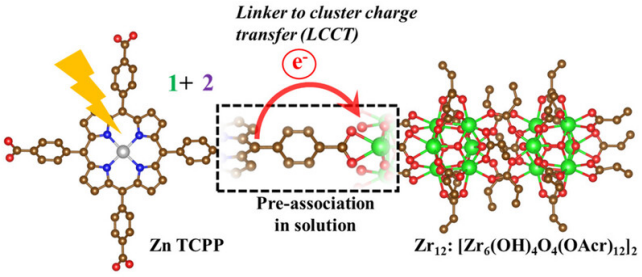


Figure 4. Photophysical processes that occur after the irradiation of Zn-TCPP remain with Zr_6-oxo cluster in homogenous solution. The Zn, C, N, O, and Zr are shown as white, brown, blue, red, and green circles, respectively. Hydrogen atoms are omitted for clarity. Reproduced from open access Ref. [43].

In another example, ultrathin two-dimensional PMOF nanosheets were constructed by coordinating Pd-metalated TCPP (Pd-TCPP) linkers to Cu (II) paddle-wheel nodes ($Cu_2(COO)_4$) (Figure 5). In this system, the Cu-based SBUs were essential for directing the formation of the 2D nanosheet morphology and promoting interfacial charge transfer. The enhanced hydrogen evolution performance was attributed to the long-lived charge-separated states of the Pd-porphyrin units combined with the reduced charge-transport distances inherent to the ultrathin nanosheet architecture [44].

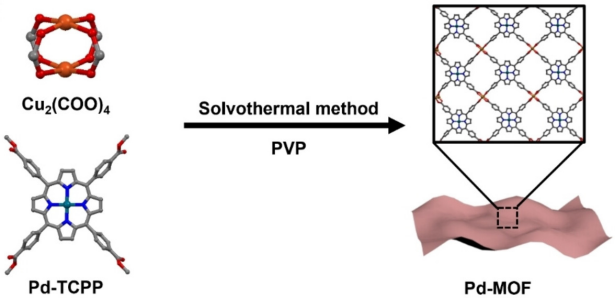


Figure 5. Schematic illustration of synthesis of Pd-MOF nanosheets. Reproduced from open access Ref. [44].

2.4. Impact of Porphyrin Metal Center in PMOFs

The nature of the metal center embedded within the porphyrin macrocycle plays a decisive role in governing the photophysical properties, excited-state lifetimes, and redox behavior of TCPP-based photocatalysts. However, the influence of the porphyrin metal must be evaluated within a constant structural framework, as variations in inorganic nodes, framework dimensionality, and overall MOF topology (e.g., 2D versus 3D architectures) can independently and strongly affect charge separation and hydrogen evolution activity. Consequently, comparisons across structurally unrelated MOFs often lead to misleading conclusions, whereas intra-framework comparisons where only the porphyrin metal center is varied provide meaningful mechanistic insights.

A clear example of such a controlled comparison was reported by Kim et al., who directly evaluated Pd-TCPP and Pt-TCPP linkers within an identical ultrathin 2D MOF nanosheet architecture featuring Cu (II) paddle-wheel nodes. Under identical irradiation conditions, the Pd-TCPP-based MOF achieved a hydrogen evolution rate of 21.3 $mmol \cdot g^{-1} \cdot h^{-1}$, substantially outperforming the Pt analog, which exhibited a rate of 6.6 $mmol \cdot g^{-1} \cdot h^{-1}$ (Entry 3, Table 1). Time-resolved spectroscopic studies attributed the superior activity of the Pd-containing framework to the formation of longer-lived charge-separated states, arising from enhanced stabilization of the triplet excited state via heavy-atom effects associated with Pd [44]. The critical role of the porphyrin metal center was further demonstrated by Chen et al., who investigated the incorporation of Cu^{2+}, Co^{2+}, and Ni^{2+} ions into the porphyrin cores of an otherwise identical 2D Ti-based PMOF. Among the series, Cu-PTM exhibited a hydrogen evolution rate of 5.465 $mmol \cdot g^{-1} \cdot h^{-1}$ approximately 27 times higher than that of the metal-free PMOF (Entry 4, Table 1). In contrast, the Co- and Ni-containing analogs produced only trace amounts of H_2. Spectroscopic analyses revealed that Cu^{2+} acts as a transient catalytic center, facilitating proton-reduction kinetics while preserving the structural integrity of the framework. These performance differences were rationalized by the distinct photophysical behavior of the metal centers: Cu^{2+} promotes ligand-to-metal charge transfer (LMCT) and long-lived charge-transfer states, whereas Co^{2+} and Ni^{2+} introduce low-lying d orbitals that rapidly quench excited states, thereby suppressing effective HER activity [45].

Consistent trends were observed in a series of Ti-based MOF nanostructures (TMF-M, M=Zn, Co, Cu) synthesized via a one-pot coordination-driven strategy. Among these materials, TMF(Zn) displayed the highest photocatalytic performance, achieving a hydrogen evolution rate of 3.24 $mmol \cdot g^{-1} \cdot h^{-1}$ under visible-light irradiation, approximately 2.3 times higher than that of the parent TMF framework (Entry 5, Table 1). This enhanced activity was attributed to the favorable optical response and optimal band-gap alignment introduced by Zn^{2+} incorporation into the porphyrin core [40].

Further insight into metal-center effects was provided by Mandal et al., who prepared a series of disordered $Zr_6O_4(OH)_4$-based PMOFs (PCN-221-M) incorporating metalloporphyrin linkers M-TCPP (M=2H, Zn^{2+}, Ni^{2+}, and a 1:1 Zn^{2+}/Ni^{2+} mixture) [43]. Among these, PCN-221(Zn) exhibited the highest HER rate of 0.2 $mmol \cdot g^{-1} \cdot h^{-1}$, followed by PCN 221 at 0.14 $mmol \cdot g^{-1} \cdot h^{-1}$. In contrast, Ni-containing frameworks showed a markedly reduced activity, with PCN-221(Ni) yielding only 0.013 $mmol \cdot g^{-1} \cdot h^{-1}$, while the mixed-metal PCN 221 (ZnNi) achieved an intermediate rate of 0.073 $mmol \cdot g^{-1} \cdot h^{-1}$ (Entry 6, Table 1). The superior performance of PCN 221 (Zn) was attributed to its favorable absorption characteristics and excited-state properties, which facilitate efficient charge separation, charge transfer, and coordination of the sacrificial electron donor (TEOA). Conversely, incorporation of Ni^{2+} significantly diminished HER activity. The unexpectedly reduced performance of PCN-221(ZnNi) suggests the presence of additional excited-state deactivation pathways, likely arising from inter-porphyrin electron transfer between Zn- and

Ni-centered units and enhanced nonradiative decay processes. Mechanistically, photocatalytic H_2 evolution in PCN-221(Zn) proceeds via two parallel pathways (Figure 5). One pathway involves electron transfer from photoexcited Zn-TCPP ligands to the SBU, which act as catalytic centers, while the second pathway arises from direct participation of the Zn-TCPP photosensitizers through their stepwise reduction to chlorin and bacteriochlorin intermediates. This dual-channel mechanism synergistically enhances hydrogen evolution efficiency and highlights the intricate interplay between porphyrin metal centers, framework nodes, and excited-state dynamics.

When evaluated under identical light-driven conditions within a structurally uniform framework, clear and consistent trends emerge regarding the influence of the porphyrin metal center on photocatalytic performance. PMOFs incorporating Zn^{2+}, Cu^{2+}, Pd^{2+}, or Pt^{2+} generally exhibit significantly higher H_2 evolution activities, whereas frameworks containing Co^{2+} or Ni^{2+} display markedly limited performance. These trends originate from the distinct ways in which different metal centers modulate the electronic structure and excited-state dynamics of the porphyrin macrocycle. Closed-shell Zn^{2+} ions (d^{10}) and heavier Pd^{2+}/Pt^{2+} ions (d^8) favor the formation of long-lived excited states by suppressing nonradiative deactivation pathways. In Zn-based PMOFs metalation raises the energy of the porphyrin π^* orbital, effectively lowering the conduction-band edge and enhancing both the thermodynamic driving force for proton reduction and the efficiency of charge separation. In contrast, Co^{2+}- and Ni^{2+}-based frameworks consistently exhibit poor photocatalytic activity. Their open-shell electronic configurations introduce low-lying metal-centered d orbitals that efficiently quench porphyrin excited states, thereby inhibiting charge separation and accelerating nonradiative decay. As a result, ligand-to-metal charge transfer (LMCT) is ineffective, long-lived charge-separated states do not form, and hydrogen evolution remains negligible despite otherwise identical structural and experimental conditions. Collectively, these findings underscore that the identity of the porphyrin metal center is a decisive factor governing excited-state lifetimes, LMCT efficiency, and the thermodynamic feasibility of H_2 evolution, but only when assessed within a single, well-defined framework. Such intra-system comparisons are essential to avoid misleading correlations between metal identity and catalytic performance that can arise when comparing structurally disparate MOF families, where variations in SBUs, electronic coupling, and morphology can independently dominate photocatalytic behavior.

2.5. Enhancement of H_2 Evolution Kinetics

The kinetics of photocatalytic hydrogen evolution in PMOFs are ruled not only by the intrinsic photophysics of the porphyrin linker, the SBU, and the metal center, but crucially also by the morphology of conventional photocatalysts and metal doping. Among the most effective strategies for accelerating HER kinetics is the integration of platinum nanoparticles (Pt NPs) into PMOF architectures. Pt NPs/PMOFs consistently exhibit enhanced hydrogen evolution activity, primarily due to Schottky barrier formation at the MOF-Pt interface, which promotes efficient charge separation and directional electron transfer. Pt NPs can be incorporated into PMOFs through several approaches, including the introduction of pre-synthesized nanoparticles with controlled sizes, either embedded within the framework pores or immobilized on the external surface. Alternatively, in situ encapsulation strategies enable the formation of Pt NPs inside the internal cavities. This intimate spatial arrangement allows photoexcited electrons, generated on the porphyrin ligands and transferred to the metal clusters via LMCT, to be rapidly extracted by Pt NPs through the Schottky junction. As a result, charge recombination is suppressed and HER kinetics are significantly accelerated.

An illustrative example of this synergistic effect was reported in a system combining controlled in situ reduction in porphyrin-embedded single Pt atoms to generate highly dispersed metallic nanoparticles within ultrathin 2D PMOF channels. This architecture delivered one of the highest reported hydrogen evolution rates, reaching 33.19 mmol·g^{-1}·h^{-1} (Entry 7, Table 1). The exceptional performance was attributed to the coexistence of dual electron-transfer pathways: Pt nanoparticles facilitate rapid electron extraction via Schottky junctions, while monatomic Pt species embedded within the porphyrin framework enable ligand-to-linker metal charge transfer (LLCMT), thereby enhancing charge separation and overall HER activity [46].

Morphological engineering further plays a pivotal role in enhancing HER kinetics. Ultrathin PMOF nanosheets effectively suppress bulk charge recombination by shortening electron and hole diffusion lengths and maximizing the surface density of catalytically active porphyrin units. Wang et al. synthesized ultrathin porphyrin-Ti MOF nanosheets via a solvothermal approach, yielding few-layer 2D architectures. Upon photodeposition of Pt nanoparticles as cocatalysts, the resulting ultrathin PMOF exhibited a high H_2 evolution rate of 8.52 mmol·g^{-1}·h^{-1} under broad visible irradiation up to approximately 700 nm (Entry 8, Table 1). Compared to bulk PMOF counterparts, this enhanced activity was ascribed to improved charge transport, stronger LMCT from porphyrin ligands to Ti-oxo clusters, and more efficient charge extraction in the thin-sheet morphology. Collectively, these effects result in higher active-site exposure and improved coupling to cocatalysts or single-atom sites [47].

Except for nanoparticle-based cocatalysts, the stabilization of single metal atoms within PMOFs represents an approach to maximize atom efficiency and fine-tune HER kinetics. Embedding single metal atoms (Pt, Ir, Au, Ru, etc.) into pore-confined nanospaces stabilizes atomically dispersed catalytic centers while preventing aggregation. Mo et al. developed a "precoordination-confinement" strategy to introduce single metal atoms (M = Pt, Ir, Au, Ru, etc.) into the pore nanospaces of Pd-PCN-222, a Zr-based PMOF featuring Pd-TCPP linkers and Zr-oxo clusters arranged in nanorod or nanotube morphologies (Figure 6). The resulting M-SAs@Pd-PCN-222 materials exhibited high hydrogen evolution activity, with reported rates up to 16.591 μmol·g^{-1}·h^{-1} (Entry 9, Table 1), along with large TONs, and excellent cycling stability. The enhanced kinetics were rationalized by the presence of atomically precise catalytic sites that maximize metal utilization, confinement effects that stabilize favorable coordination environments (e.g., Pt-N_2O_2 motifs), and improved adsorption and activation of water and proton-reduction intermediates. Together, these factors lower the apparent hydrogen adsorption free energy ΔGH* and accelerate the overall HER process [48].

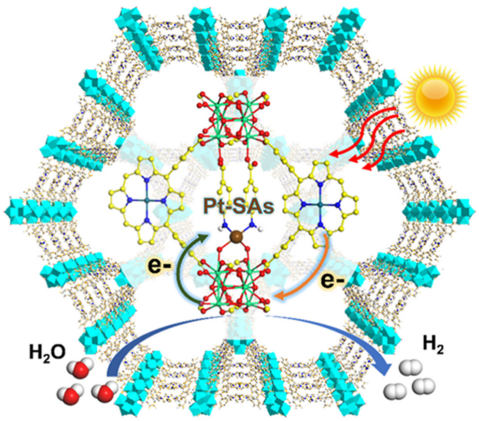


Figure 6. Schematic illustration of the structure and photocatalytic behavior of Pt-SAs@Pd-PCN-222-NH_2. Color of elements: H, white; O, red; C, yellow; N, blue; Zr, cyan; and Pt, brown. Reproduced from [48] with permission from American Chemical Society, License number 6174811223935.

Recently, a platinum–porphyrin–zirconium MOF, PCN-223(Pt), was synthesized via the self-assembly of PtTCPP ligands and Zr_6 clusters. In this system, Pt ions were pre-coordinated to the nitrogen atoms of the porphyrin cores prior to framework formation, resulting in a uniform and well-defined distribution of Pt catalytic sites throughout the MOF architecture. The resulting PCN-223(Pt) exhibited a hydrogen evolution rate of 0.732 $mmol \cdot g^{-1} \cdot h^{-1}$ corresponding to a 7.6-fold enhancement relative to the parent PCN-223 framework (Entry 10, Table 1). This pronounced improvement was attributed to efficient electron transfer from photoexcited porphyrin units to the Pt centers, which act as catalytic sites for proton reduction, as well as to enhanced separation of photogenerated charge carriers enabled by the homogeneous dispersion of Pt within the framework [49].

Also, Lin et al. developed a series of Zr_6-PMOF PCN-H_2/Ptx:y containing different ratios of metal-free H_2TCPP and Pt^{II}TCPP, where x:y = 0:1, 2:3, 3:2, and 4:1 (Figure 7). Among this series, PCN-H_2/$Pt_{0:1}$ exhibited the highest photocatalytic H_2 evolution activity (0.351 $mmol \cdot g^{-1} \cdot h^{-1}$) (Entry 11, Table 1). This enhanced performance was attributed to the uniform dispersion of Pt (II) ions within the porphyrin cores, which enables efficient charge transfer from the porphyrin photosensitizers to the Pt(II) catalytic centers. Such intimate electronic coupling promotes effective charge separation and suppresses recombination within the MOF framework, thereby enhancing overall HER efficiency [33].

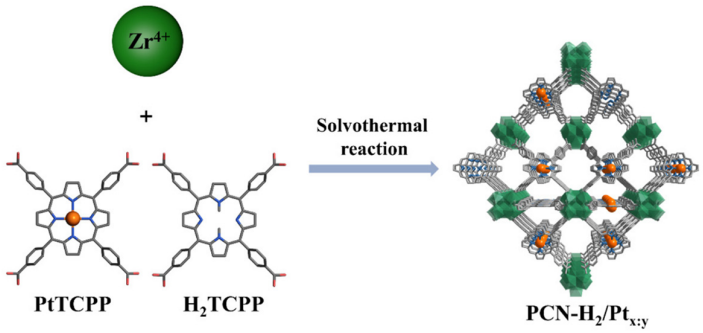


Figure 7. Synthesis of PCN-H_2/$Pt_{x:y}$ (x:y = 0:1, 2:3, 3:2, and 4:1). Reproduced from [33] with permission from American Chemical Society, License number 6174820207995.

Additionally, a novel bimetallic photocatalyst Pd/Yb-PMOF showed how secondary-metal incorporation can effectively tune optical absorption and charge carrier dynamics (Figure 8). Under visible-light irradiation and in the presence of 2 wt% Pt as a co-catalyst, this bimetallic PMOF achieved an enhanced hydrogen evolution rate of up to 3.196 $mmol\ g^{-1} \cdot h^{-1}$ (Entry 12, Table 1). The improved photocatalytic performance was attributed to the coexistence of diverse metal active sites, favorable band-gap alignment, strong visible-light-harvesting capability, efficient charge-carrier transfer, and a pronounced synergistic interaction between Yb and Pd ions within the framework [50].

Leng et al. reported a distinctive strategy for enhancing photocatalytic H_2 evolution in PMOFs that departs from conventional isostructural metalated frameworks. In this work, an indium-based MOF, denoted USTC-8(In), was synthesized from In–oxo chain nodes and H_4TCPP linkers (Figure 9). Unlike traditional metalloporphyrin systems, in which the metal ion resides within the porphyrin plane, the In^{3+} ions in USTC-8(In) adopted an out-of-plane (OOP) coordination geometry due to their larger ionic radius. This unconventional metal coordination mode proved highly advantageous for visible-light-driven H_2 production. Under visible-light irradiation and in the presence of Pt as a cocatalyst, USTC-8(In) achieved a hydrogen evolution rate of 0.341 $mmol \cdot g^{-1} \cdot h^{-1}$ corresponding to an enhancement of up to 37-fold relative to the in-plane metalated analogs USTC-8(Co), USTC-8(Ni), and USTC-8(Cu) (Entry 13, Table 1). This pronounced performance improvement was attributed to prolonged charge-separated states and effective suppression of rapid back-electron

transfer from the metal center to the porphyrin macrocycle, underscoring the critical role of metal coordination geometry in modulating excited-state dynamics [51].

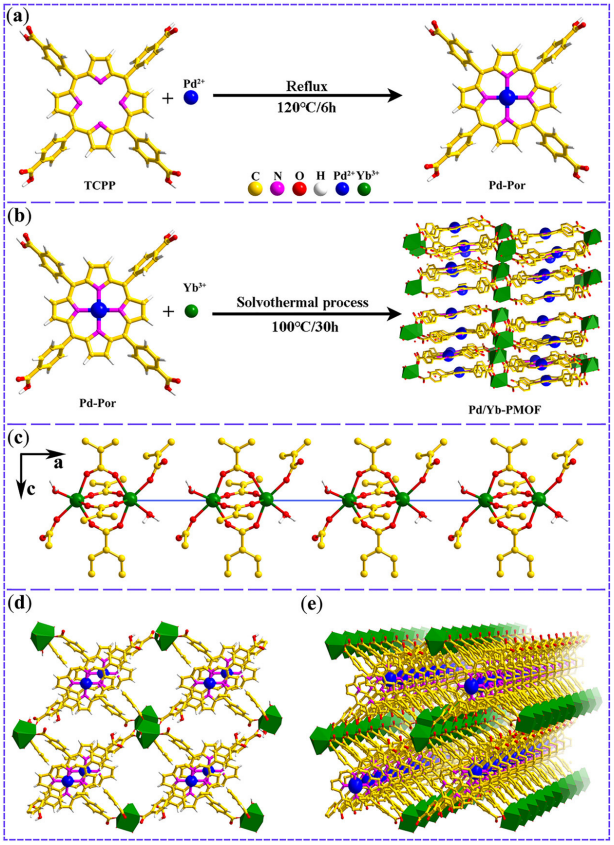


Figure 8. Schematic diagram of the synthesis process for (**a**) Pd-Por and (**b**) Pd/Yb-PMOF. (**c**) Chain structures of $Yb_2O_{10}(OH_2)_2$ along the a-axis for Yb-PMOF and Pd/Yb-PMOF, (**d**) visual representation of 1D pore channels, and (**e**) 3D framework structures of Pd/Yb-PMOF. Reproduced from [50] with permission from the American Chemical Society, License number 6174820438683.

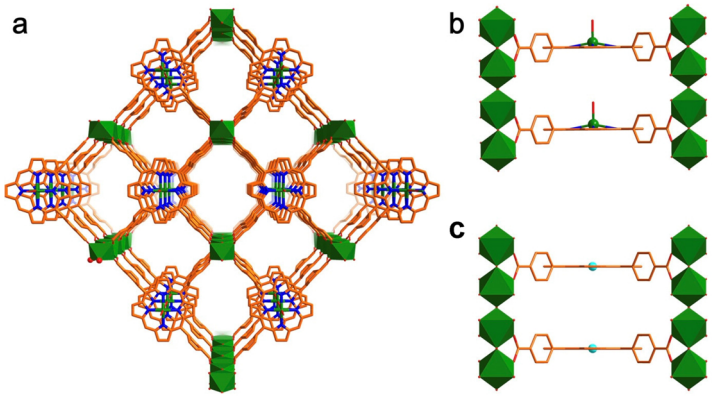


Figure 9. (**a**) View of the 3D network of USTC-8(In) along an axis. Views of partial structures in (**b**) USTC-8(In) and (**c**) USTC-8(M) (M = Cu, Co, Ni), highlighting the metal location at the metalloporphyrin motif involved in the MOF structure. The framework is represented by a wire model, and the metal atoms at metalloporphyrins are represented by a ball-and-stick model. The $InO_4(OH)_2$ polyhedra are shaded in olive green. The In, Cu, C, O, and N are shown as green, cyan, orange, red, and blue circles, respectively. Hydrogen atoms are omitted for clarity. Reproduced from [51] with permission from the American Chemical Society, license number 6174820910669.

2.6. Current Limitations of PMOFs

Porphyrinic MOFs have emerged as highly promising photocatalysts for visible-light-driven hydrogen evolution; nevertheless, several critical challenges must be addressed before their practical implementation can be realized. First, photochemical and hydrolytic stability under operating conditions remain a significant concern. Despite exhibiting high initial activities, many PMOFs suffer from partial loss of crystallinity, linker degradation, or diminished catalytic performance after prolonged irradiation in aqueous or protic media. These stability issues underscore the importance of stability-oriented design strategies, particularly the use of robust metal–oxo secondary building units such as Zr-based clusters, which are known to impart enhanced resistance against hydrolysis and photodegradation [27].

Second, bulk recombination and limited charge-separation efficiency in micro-sized PMOF crystals frequently suppress external quantum efficiencies. In such systems, long charge-transport distances and insufficient interfacial extraction pathways lead to rapid recombination of photogenerated electron–hole pairs. Experimental studies have demonstrated that this limitation can be mitigated through morphological engineering, including the development of ultrathin or few-layer PMOF nanosheets, as well as through the construction of intimate heterojunctions with complementary semiconductors or conductive phases. These approaches significantly enhance hydrogen evolution rates compared with their bulk counterparts by shortening charge-migration pathways and promoting efficient charge extraction [52].

Finally, the continued reliance on noble metal cocatalysts, particularly Pt and Pd, remains a major bottleneck for large-scale applications. Although such cocatalysts are highly effective in accelerating proton-reduction kinetics, their high cost, limited availability, and often substantial loading requirements raise serious concerns regarding economic viability and scalability. This challenge has stimulated growing interest in the development of earth-abundant alternatives, as well as in the stabilization of atomically dispersed metal sites within porphyrinic frameworks to maximize atom efficiency while minimizing precious-metal content [25].

Table 1. Photocatalytic performance of PMOFs for H_2 production.

Entry	PMOF Name	SED (C)/Co-Catalyst (C)	Light Source	Irradiation Time (h)	H_2 Production Rate ($mmol \cdot g^{-1} \cdot h^{-1}$)	Ref.
1	TCPP-Zn-BTDO	AA (0.2)/Pt (3 wt%)	$\lambda > 400$ nm 300 W Xe lamp	--	1.48	[37]
2	TMF-Pt	AA (1 M)/Pt	$\lambda \geq 420$ nm 300 W Xe lamp	--	15.5	[41]
3	Pd-MOF	--/Pd	$\lambda = 450$ nm, 500 mW/cm^2	3 h	21.3	[44]
	Pt-MOF	--/Pt			6.6	
4	Cu-PTM	TEOA	$\lambda \geq 420$ nm 300 W Xe lamp	--	5.465	[45]
5	TMF	TEOA (10% *v*/*v*)/Pt	$\lambda \geq 420$ nm 300 W Xe lamp	6 h	1.42	[40]
	TMF(Zn)				3.240	
6	PCN 221	TEOA/--	405 nm LED source (900 mW)	24 h	0.14	[43]
	PCN 221 Zn				0.2	
	PCN 221 Ni				0.013	
	PCN 221 ZnNi				0073	
7	TMF-Pt/Pt NPs	TEOA/Pt single atoms + Pt NPs (in situ)	$\lambda > 400$ nm 300 W Xe lamp	5 h	33.19	[46]

Table 1. *Cont.*

Entry	PMOF Name	SED (C)/Co-Catalyst (C)	Light Source	Irradiation Time (h)	H_2 Production Rate ($mmol \cdot g^{-1} \cdot h^{-1}$)	Ref.
8	Pt@PMOF	AA (10 mmol)/Pt NPs (3 wt%)	$\lambda > 400$ nm 300 W Xe lamp	5 h	8.52	[47]
9	Pt-SA@Pd-PCN-222-NH_2	Triisopropanolamine (5.24 mmol)/Pt	$\lambda \geq 400$ nm 300 W Xe lamp	3 h	16.59	[48]
10	PCN-223(Pt)	TEOA/Pt-metallation	$\lambda \geq 400$ nm 300 W Xe lamp	--	0.732	[49]
11	PCN-H_2/$Pt_{0:1}$	TEOA/Pt	$\lambda > 400$ nm 300 W Xe lamp	16 h	0.351	[33]
12	Pd/Yb-PMOF	TEOA (0.1 M)/Pt (2 wt%)	$\lambda \geq 420$ nm 300 W Xe lamp	5 h	3.196	[53]
13	USTC-8(In)	Triethylamine/Pt (1.5 wt%)	$\lambda > 380$ nm 300 W Xe lamp	--	0.341	[51]

3. Porphyrinic Covalent Organic Frameworks (PCOFs) for H_2 Evolution

Covalent organic frameworks (COFs) possess several intrinsic features that render them highly attractive platforms for the rational design of efficient photocatalysts [54–56]. Their long-range ordered structures and extended π–π conjugation networks promote exposure of photoactive sites, broaden light-absorption windows, and facilitate the migration of photoinduced excitons. Owing to their π-conjugated electronic structures, most COFs exhibit suitable energy-level alignment and moderate band gaps that enable efficient visible-light response. Importantly, band-gap engineering can be readily achieved at the molecular level through judicious selection of monomers, modulation of conjugation length, or introduction of electron-donating and electron-withdrawing functional groups. As a result, the optical and electronic properties of COFs can be precisely tailored, highlighting their exceptional structural tenability and potential for high photocatalytic performance [57]. The PCOFs further enhance these advantages by combining the strong visible-light absorption, long-lived excited states, and rich redox chemistry of porphyrins with the permanent porosity and structural order of COFs. Consequently, PCOFs have emerged as a versatile and rapidly growing class of photocatalysts for solar-driven hydrogen evolution.

3.1. Structural Design Principles in PCOFs

A range of complementary design strategies can be employed to achieve high photocatalytic activity and efficient hydrogen evolution in PCOFs. Incorporation of porphyrin units into COF architectures significantly broadens the light-absorption range and enhances photochemical and photophysical properties, thereby expanding the scope of visible-light-driven applications. In studies of PCOFs for photocatalytic H_2 production, metalation of the porphyrin core, as well as the introduction of additional metal-containing catalytic sites, is frequently used to boost photocatalytic performance by tuning excited-state lifetimes and redox potentials [58]. Owing to the inherent C4 symmetry of porphine and its derivatives, most reported PCOFs adopt one-dimensional or two-dimensional network structures. Nevertheless, through careful selection of appropriately functionalized porphyrin building blocks and complementary linkers, it is possible to construct highly ordered PCOFs with robust covalent bonds and tailored topological arrangements, including more complex or higher-dimensional architectures [59]. Such structural control is essential for optimizing light harvesting, charge separation, and catalytic site accessibility.

Functional-group engineering represents another effective method to enhance photocatalytic efficiency. Introducing electron-donating or electron-withdrawing groups can

create internal charge traps that facilitate excitation, promote charge separation, and suppress electron–hole recombination. In parallel, the photocatalytic performance of PCOFs is strongly influenced by their porous architecture. Rational tuning of pore size, shape, and connectivity provides abundant accessible catalytic sites and enables uniform distribution of photosensitizers and cocatalysts throughout the framework. This structural optimization improves mass transport, reduces the migration distance of photogenerated charge carriers, and facilitates efficient diffusion of reactants and products, collectively enhancing hydrogen evolution kinetics [60]. Donor–acceptor (D-A) architecture plays a particularly critical role in determining photocatalytic activity. By spatially separating electron-rich and electron-deficient moieties within the framework, D-A PCOFs promote efficient charge separation, accelerate exciton dissociation, and effectively suppress recombination losses, leading to markedly improved photocatalytic performance [61]. Finally, additional structural factors including interlayer stacking mode, crystallinity, hydrophilicity, and overall stability must be carefully considered in PCOF design. High crystallinity facilitates rapid transport of photogenerated electrons and holes to reactive surface sites, while minimizing recombination. During COF synthesis, crystallinity is governed by multiple parameters, among which solvent choice plays a dominant role [62]. Adequate chemical and photochemical stability are essential to prevent framework degradation during prolonged illumination and catalytic operation. Appropriate hydrophilicity enhances interfacial contact with aqueous media, further promoting photocatalytic hydrogen evolution [63]. Collectively, precise structural control not only deepens mechanistic understanding of structure-property relationships in PCOFs but also enables the rational development of highly efficient photocatalysts tailored for solar hydrogen production [12].

3.2. Influence of Linker Functionalization and Functional Groups of PCOFs

The synthesis of PCOFs is typically based on condensation reactions between monomers bearing complementary reactive functional groups, enabling the construction of extended crystalline networks with well-defined connectivity (Figure 10).

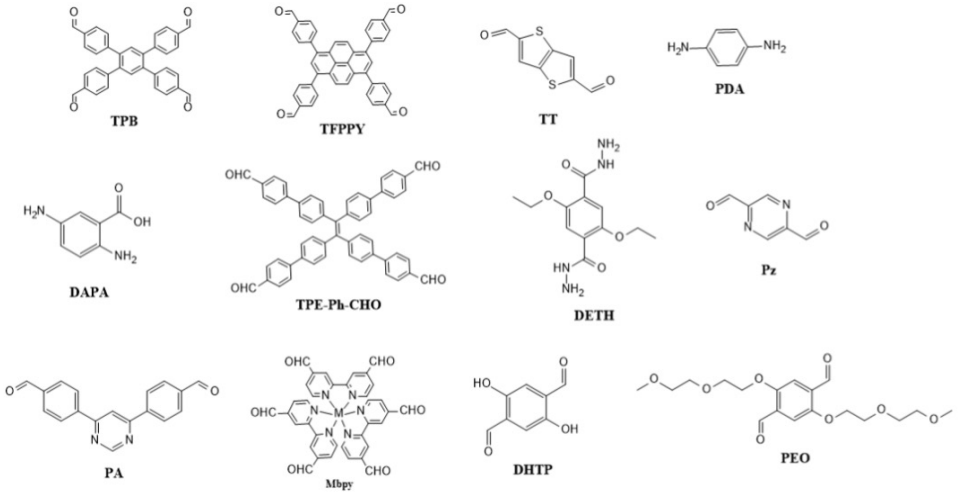


Figure 10. Recent linkages used for the development of PCOFs.

Common synthetic routes involve the reaction of 5,10,15,20-tetrakis(4-aminophenyl)-21H,23H-porphyrine (TAPP) with various aldehyde-bearing linkers or alternatively 5,10,15,20-tetrakis(4-formylphenyl) 21H,23H porphyrin (TFPP) with amine-bearing linkers. COFs are constructed from repeating units linked through robust covalent bonds, such as imines, hydrazones, among others. These linkages serve as structural bridges that establish long-range connectivity across the framework, imparting both structural stability and

tunable chemical functionality to the resulting COFs. Among these, imine-linked COFs are the most extensively studied photocatalysts owing to the facile formation of reversible imine bonds via Schiff-base condensation between amines and aldehydes.

Functional-group engineering represents an additional strategy for modulating the electronic structure of PCOFs and enhancing charge separation and migration. Introducing polar functional groups can tune electron density distributions within the framework and strengthen interactions with aqueous media. Song and coworkers demonstrated this principle by incorporating carboxyl groups into the linker of a PCOF, as it exhibits high polarity and strong affinity to water (Figure 11) [58]. The Por-COOH-COF achieved a HER rate of 12.773 mmol·g^{-1}·h^{-1}, nearly four times higher than that of the unmodified Por-COF (3.351 mmol·g^{-1}·h^{-1}) (Entry 1, Table 2). Density functional theory calculations combined with in situ X-ray photoelectron spectroscopy revealed that carboxyl functionalization promotes charge transfer from the porphyrin core to the imine (–C=N–) linkages under UV-Visible irradiation, accounting for the significantly enhanced photocatalytic performance.

Extended π-conjugation within linker units further plays a decisive role in determining photocatalytic activity. Pyrene-based COFs have attracted substantial interest owing to their strong visible-light absorption and efficient exciton delocalization [9]. Liu et al. synthesized two imine-linked 2D PCOFs TPB-TAPP-COF and TFPPY-TAPP-COF to investigate the effect of donor conjugation on hydrogen evolution (Figure 12) [63]. Using the same porphyrin amine acceptor, TFPPY-TAPP-COF, which incorporates a pyrene-based donor with higher π-electron density and improved coplanarity, exhibited superior performance. With 5 wt% Pt as a cocatalyst, TFPPY-TAPP-COF achieved a hydrogen evolution rate of 8.7 mmol·g^{-1}·h^{-1}, nearly twice that of TPB-TAPP-COF (4.2 mmol·g^{-1}·h^{-1}) (Entry 2, Table 2). This enhancement was attributed to stronger donor-acceptor interactions, reduced band-gap energy, improved electron delocalization, and more efficient charge separation.

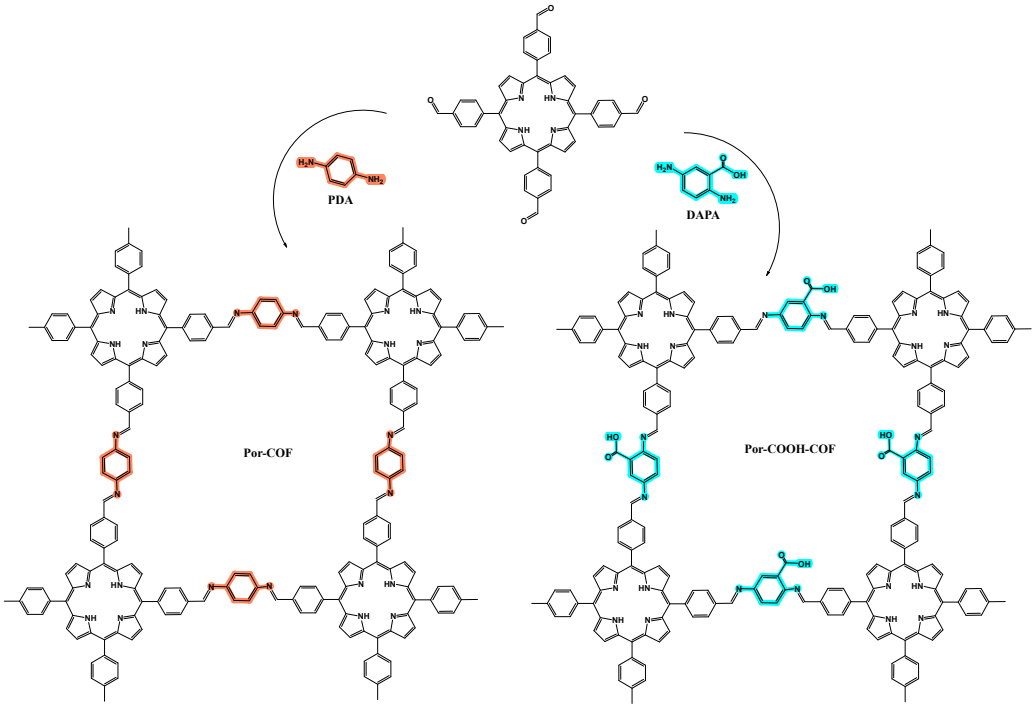


Figure 11. Synthetic route of Por-COF and Por-COOH-COF.

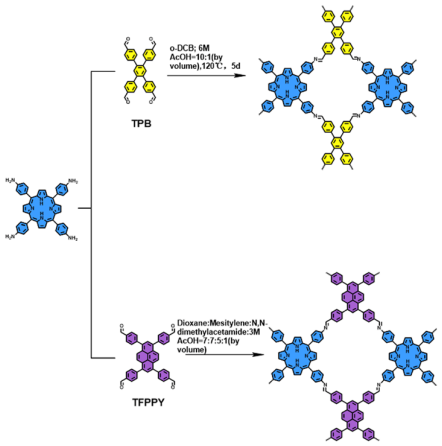


Figure 12. Experimental preparation of TPB-TAPP-COF and TFPPY-TAPP-COF. Reproduced from [63] with permission from the Royal Society of Chemistry, license number 1685221-1.

Nitrogen-rich heterocycles offer another effective means of tuning electronic structure and charge-transport properties. He et al. developed three-component PCOFs incorporating either pyrazine or phenyl linkers to create π-conjugated photocatalysts for hydrogen production (Figure 13). Post-synthetic modification of the pyrazine sites enhanced active-site anchoring, hydrophilicity, and electron transport [64]. The incorporation of pyrazine units introduces abundant C=N groups that facilitate proton transport via hydrogen bonding, while simultaneously narrowing the band gap and suppressing electron-hole recombination. Collectively, these effects lead to markedly improved photocatalytic efficiency [65].

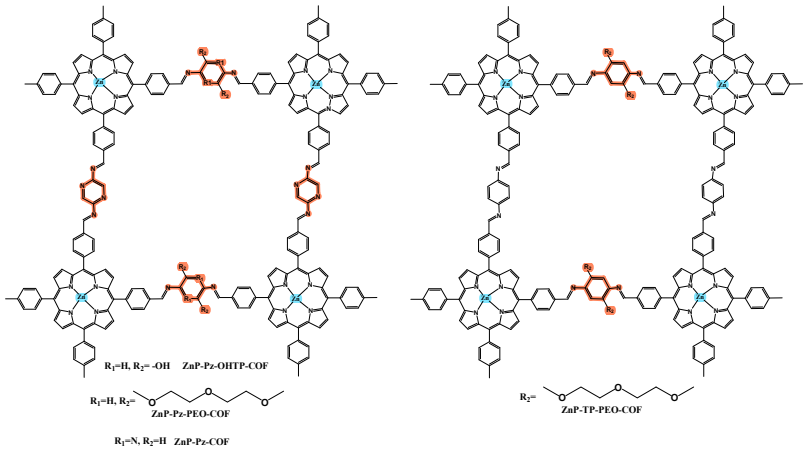


Figure 13. Three-component porphyrin-based COFs incorporating either N-rich pyrazine or phenyl linkers to create π-conjugated photocatalysts for hydrogen production.

The pyrimidine-containing heterocycles have also emerged as highly effective electron-accepting motifs for photocatalytic hydrogen evolution. Huan et al. reported the design of a one-dimensional PCOF, TP-PA-COF, constructed from a non-metallic porphyrin monomer (TP) and a pyrimidine carboxaldehyde linker (PA) (Figure 14). This framework exhibits high crystallinity and a well-defined microporous network that facilitates efficient mass transport. Under visible-light irradiation, TP-PA-COF demonstrated outstanding photocatalytic performance, achieving a hydrogen evolution rate of up to 37.4 $mmol \cdot g^{-1} \cdot h^{-1}$ (Entry 3, Table 2), highlighting the effectiveness of strong electron-accepting heterocycles in promoting charge separation and HER kinetics [66].

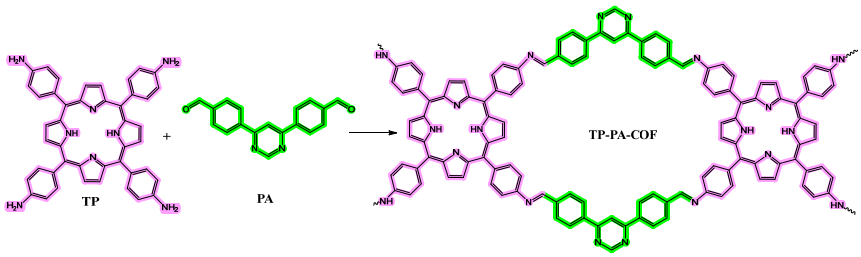


Figure 14. Schematic diagram of the synthesis of TP-PA-COF.

Hydrazone-based PCOFs have gained increasing attention due to their superior chemical robustness. For example, Chen et al. synthesized a series of isostructural MPor-DETH-COFs (M = H_2, Co, Ni, Zn) by condensing porphyrinic aldehydes (MPor-CHO) with 2,5-diethoxyterephthalohydrazide (DETH) [67]. All four frameworks adopt AA-stacked structures with high crystallinity and large surface areas, exhibiting enhanced hydrolytic resistance relative to imine-linked analogs due to extended π–π conjugation between nitrogen and carbonyl groups.

A wide variety of electron-donating and electron-accepting aldehyde linkers have also been coupled with TAPP to generate structurally diverse porphyrinic COFs. Xu et al. synthesized TAPP-TBPE via Schiff-base condensation between TAPP and 1,1,2,2-tetra(4-formyl-(1,1′-biphenyl)) ethene (TPE-Ph-CHO). The resulting TP-COF exhibited a hydrogen evolution rate of 0.0584 mmol·g^{-1}·h^{-1}, which was attributed to efficient fluorescence resonance energy transfer (FRET) from tetraphenylethylene units to the porphyrin core (Entry 4, Table 2) [68]. Similarly, Lv et al. prepared TAPPZn-TT by condensing TAPPZn with thieno [3,2-b] thiophene-2,5-dicarbaldehyde, in the presence of Pt and ascorbic acid as a sacrificial agent; this COF achieved a hydrogen evolution rate of 8.2 mmol·g^{-1}·h^{-1} (Entry 5, Table 2) [69].

Notably, Lu et al. demonstrated that three-dimensional PCOF architectures can further enhance photocatalytic performance by increasing active-site density and accelerating substrate diffusion relative to conventional 2D stacked structures. By reacting hexaformyl-functionalized $Ru(bpy)_3$ or $Fe(bpy)_3$ complexes with MTAPP (M = H_2 or Zn), they constructed the 3D frameworks TAPPM-Rubpy and TAPPM-Febpy (Figure 15). Among these materials, TAPPZn-Rubpy exhibited exceptional activity, achieving a hydrogen evolution rate of 30.338 mmol·g^{-1}·h^{-1}, one of the highest reported values for COF-based photocatalysts (Entry 6, Table 2). This performance was approximately 31 times higher than that of Febpy-ZnPor COF and 12 times higher than that of Rubpy-2HPor COF. Density functional theory calculations revealed that both the $Ru(bpy)_3$ and Zn-porphyrin units can be photoexcited and undergo two sequential electron-transfer pathways, enabling dual excitation and significantly increasing the number of electrons participating in the photocatalytic reaction. This dual-photosensitizer mechanism greatly enhances light-to-electron conversion efficiency and drives highly efficient photocatalytic water splitting to generate H_2 [70].

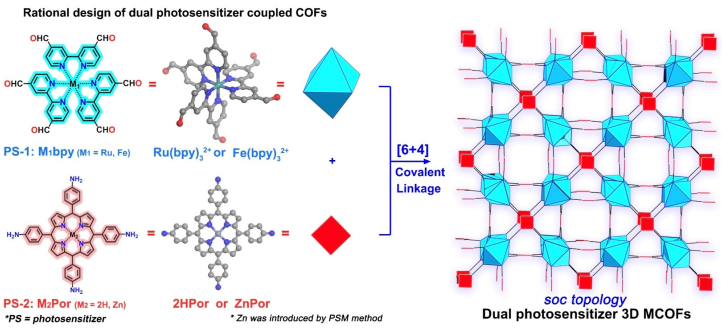


Figure 15. Schematic of the design and structure of dual photosensitizer 3D MCOFs and the constructed topology. Reproduced from [70] with permission from Wiley, license number 6174801032015.

Table 2. Photocatalytic performance of PCOFs for H_2 production.

Entry	PCOF Name	SED (C)/Co-Catalyst (C)	Light Source	Irradiation Time (h)	H2 Production Rate (mmol·g−1·h−1)	Ref.
1	Por-COOH-COF	TEOA (10%)/--	λ > 400 nm 300 W Xe lamp	3 h	12.773	[58]
	Por-COF				3.351	
2	TPB-TAPP-COF	AA/Pt (5 wt%)	420 nm	--	8.7	[63]
	TFPPY-TAPP-COF			--	4.244	
3	TP-PA-COF	AA (0.1 M)/Pt (2 wt%)	λ > 420 nm 300 W Xe lamp	12 h	37.4	[66]
4	TP COF	TEOA (20%)/Pt (5 wt%)	λ > 420 nm 300 W Xe lamp	4 h	0.058	[68]
5	TAPPZn–TT	AA (0.1 M)/Pt (5 wt%)	λ > 400 nm, xenon lamp	40 h	8.2	[69]
6	Fe(bpy)$_3$-ZnPor COF	AA/Pt	420 nm	20 h	0.9662	[70]
	Ru(bpy)$_3$-ZnPor COF				30.338	
	Ru(bpy)$_3$-2HPor COF				2.6168	
7	ZnPor-DETH-COF	TEOA/Pt (8 wt%)	λ > 400 nm 300 W Xe lamp	2–10 h	0.413	[67]
	CoPor-DETH-COF			2–10 h	0.025	
	NiPor-DETH-COF			2–10 h	0.211	
	H_2Por-DETH-COF			2–10 h	0.080	
8	TP COF	TEOA (0.85 M)/Pt (5 wt%)	λ > 420 nm 300 W Xe lamp	5 h	0.032	[71]
	Co-TP COF				0.049	
	Ni-TP COF				0.083	
	Zn-TP COF				0.141	
9	$[Mo_3S_{13}]^{2-}$@ZnP-Pz-PEO-COF	LA (15 vol%)/Mo (5.61 wt%)	λ > 420 nm 300 W Xe lamp	3 h	10.8	[64]
	$[Mo_3S_{13}]^{2-}$@ZnP-Pz-COF,				0.01	
	$[Mo_3S_{13}]^{2-}$@ZnP-Pz-DHTP-COF				4.7	
	$[Mo_3S_{13}]^{2-}$@ZnP-TP-PEO-COF				0.87	
10	COF/NiTCPP	AA (0.15 M)/Pt (3 wt%)	λ > 420 nm 300 W Xe lamp	5 h	29.71	[72]
	COF/PtTCPP				13.26	
	COF/CoTCPP				12.66	

3.3. Impact of Porphyrin Metal Center of PCOFs

Porphyrin macrocycles combine strong visible-light absorption with considerable structural and electronic tunability, allowing their photocatalytic properties to be finely adjusted through coordination of different metal ions at the central cavity. This metalation strategy has shown to be highly effective in porphyrinic COFs, where the identity of the metal center directly influences excited-state dynamics, charge-transport pathways, and ultimately hydrogen evolution activity. Wang and co-workers prepared a series of isostructural porphyrinic COFs, denoted MPor-DETH-COF, by incorporating different transition-metal ions (M = Co, Ni, Zn) into the porphyrin cores [67] (Figure 16i). Their results revealed a clear activity trend of Zn^{2+} > Ni^{2+} > Co^{2+} for photocatalytic hydrogen evolution. Specifically, ZnPor-DETH-COF exhibited an exceptionally high hydrogen

evolution rate of 413 mmol·g^{-1}·h^{-1}, followed by NiPor-DETH-COF (211 mmol·g^{-1}·h^{-1}), H_2Por-DETH-COF (80 mmol·g^{-1}·h^{-1}), and CoPor-DETH-COF (25 mmol·g^{-1} h^{-1}) (Entry 7, Table 2). The markedly lower activity of CoPor-DETH-COF was attributed to the electronic configuration of Co^{2+} ($3d^7$), which favors a dominant LMCT pathway that impedes effective hole migration through the porphyrin channels.

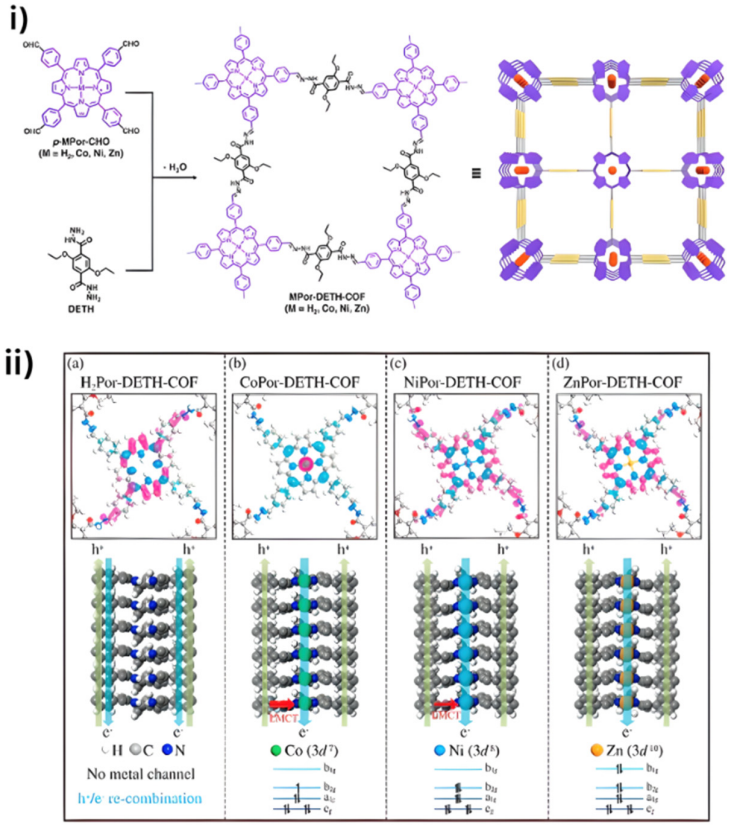


Figure 16. (**i**) Schematic representation of the synthesis of MPor-DETH-COFs. (**ii**) LMCT mechanism indicated by DFT calculations. Reproduced from open access Ref. [67].

In contrast, Ni^{2+} ($3d^8$) only partially engages in LMCT, allowing limited hole transport and intermediate photocatalytic activity. For ZnPor-DETH-COF, the closed-shell Zn^{2+} ion ($3d^{10}$) effectively suppresses LMCT, enabling photogenerated holes to migrate freely across the porphyrin π-conjugated network, while electrons are transported through Zn-Zn channels within the framework. This efficient spatial separation of charge carriers is maintained over extended timescales, leading to substantially enhanced hydrogen evolution performance (Figure 16ii). A similar enhancement effect was observed in donor–acceptor PCOF systems. For example, incorporation of Zn^{2+} into the D-A Zn-Por-TT COF resulted in a synergistic improvement in photocatalytic performance. This material exhibited an initial hydrogen evolution rate of 4.1 mmol·g^{-1}·h^{-1} during the first 5 h of irradiation, already exceeding that of its metal-free analog, and the activity continued to increase steadily, reaching 8.2 mmol·g^{-1}·h^{-1} after 10 h of illumination [69]. This behavior underscores the beneficial role of Zn^{2+} centers in promoting charge separation and sustaining long-lived reactive states.

Further insight into metal-center effects was provided by Yao et al., who synthesized a series of M-TP-COFs (M = Co, Ni, Zn) by coordinating transition-metal ions to a parent TP-COF framework [71]. Despite exhibiting similar crystallinity and porosity, these materials showed markedly different photocatalytic activities, with average hydrogen evolution rates of 0.031, 0.049, 0.084, and 0.141 mmol·g^{-1}·h^{-1}, following the trend Co-TP-COF < TP-COF <

Ni-TP-COF < Zn-TP-COF. These differences were attributed to variations in charge-carrier separation and migration kinetics induced by metal insertion.

In the metal-free TP-COF, both electrons and holes migrate through macrocycle-on-macrocycle pathways, leading to rapid recombination and short emission lifetimes. Upon metal incorporation, metal-on-metal transport channels are introduced and LMCT pathways become operative, profoundly affecting hole mobility. In Co-TP-COF, the Co^{2+} ($3d^7$) center promotes strong LMCT, severely restricting hole transport and resulting in the lowest hydrogen evolution activity. In Ni-TP-COF, the reduced LMCT contribution associated with Ni^{2+}($3d^8$) partially restores hole mobility, leading to moderate performance. In contrast, Zn-TP-COF, featuring a closed-shell Zn^{2+} ($3d^{10}$) center, suppresses LMCT altogether, enabling efficient hole migration and yielding the highest photocatalytic activity among the series.

3.4. Enhancement in H_2 Evolution Kinetics

Catalytic activity in PCOF-based photocatalysts is strongly influenced by the nature, size, and dispersion of active sites, which may range from nanoparticles to atomically dispersed species. Platinum nanoparticles embedded within COF architecture have been widely employed as highly active cocatalysts, as they provide efficient proton-reduction sites and shorten electron-transfer pathways, thereby enhancing hydrogen evolution kinetics [8]. However, the utilization efficiency of Pt nanoparticles is inherently limited, since a substantial fraction of Pt atoms remains buried within the particle core and is catalytically inaccessible. Consistent with this limitation, Liu and co-workers demonstrated that increasing Pt cocatalyst loading up to 5 wt% improved photocatalytic hydrogen production, whereas further increases led to nanoparticle agglomeration and a concomitant decline in activity [63].

Replacing noble-metal cocatalysts with earth-abundant alternatives remains a central challenge in photocatalysis. Notably, PCOFs incorporating non-noble metal cocatalysts, such as molybdenum-based clusters, have shown exceptional promise. In particular, a Zn-porphyrin–pyrazine COF decorated with $[Mo_3S_{13}]^{2-}$ clusters ($[Mo_3S_{13}]^{2-}$@ZnP-Pz-PEO-COF) containing 5.61 wt% Mo exhibited remarkably high hydrogen evolution rates, quantum yields, and turnover frequencies, in some cases surpassing those of state-of-the-art Pt-based systems [64].

To elucidate the origin of this enhanced performance, the roles of distinct interfacial environments within the COF were systematically examined. Specifically, hydrophilic pore interfaces and hydrophobic external interfaces were compared, revealing that $[Mo_3S_{13}]^{2-}$@ZnP-Pz-PEO-COF exhibits substantially higher hydrogen evolution activity at hydrophilic pore interfaces. This behavior was attributed to the facile ingress of water molecules into the accessible pore network, which enhances reactant availability at catalytic sites and accelerates proton reduction [64]. In addition, crystallinity was identified as a critical factor governing charge-carrier separation and transport. In the same study, an amorphous analog, $[Mo_3S_{13}]^{2-}$@ZnP-Pz-PEO-POP, displayed a significantly lower hydrogen evolution rate of 2.2 $mmol \cdot g^{-1} \cdot h^{-1}$, approximately five times lower than that of the crystalline COF, due to disordered π-conjugated pathways that impede efficient electron transport (Entry 9, Table 2).

Controlled aggregation of porphyrins within COF matrices offers another effective strategy for enhancing photocatalytic performance. Han et al. demonstrated that the co-assembly of metalloporphyrins (MTCPP; M=Ni, Pt, Co) onto COF surfaces is strongly dependent on the identity of the porphyrin metal center (Figure 17) [72]. The PCOF, synthesized at room temperature via Schiff-base condensation of TAPB and BTCA, exhibited markedly different hydrogen evolution activities as a function of porphyrin loading. A monolayer of NiTCPP uniformly assembled on the COF surface delivered the highest

hydrogen evolution rate, reaching 29.71 mmol·g^{-1}·h^{-1} under visible-light irradiation. In contrast, higher loadings of PtTCPP or CoTCPP led to pronounced porphyrin aggregation, which reduced light-harvesting efficiency and hindered charge transport, resulting in lower hydrogen evolution rates of 13.26 and 12.66 mmol·g^{-1}·h^{-1} for COF/PtTCPP and COF/CoTCPP, respectively (Entry 10, Table 2).

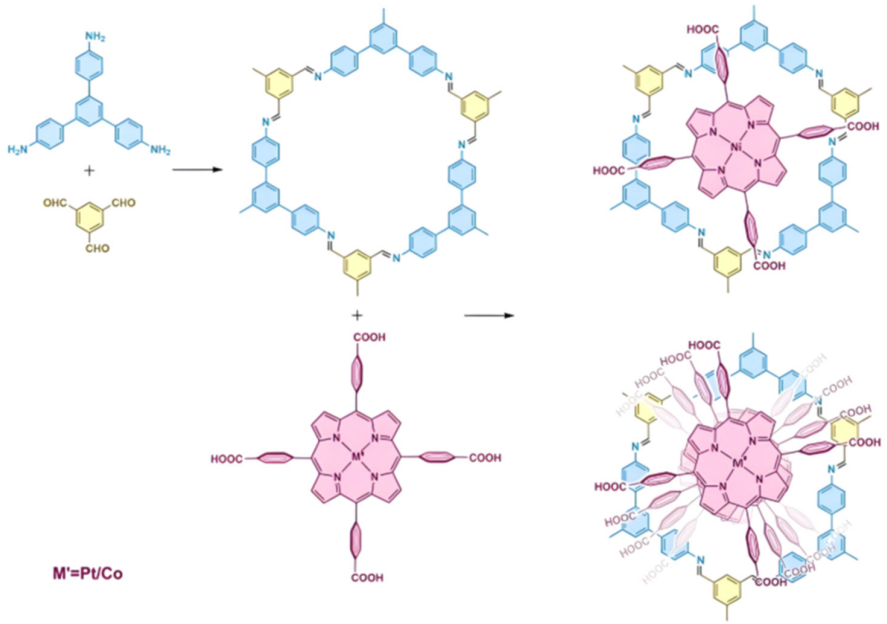


Figure 17. COF surface can be coated with porphyrin assemblies of varying thickness, depending on the metal ions in the porphyrin. Reproduced from [72], with permission from ACES, license number 6174810130385.

3.5. Current Limitations of PCOFs

Despite the encouraging H_2 evolution performance of PCOF photocatalysts, several critical challenges persist. Structural stability remains a key concern, as many COFs are prone to hydrolysis, oxidation, or photodegradation owing to reversible or chemically labile linkages [73]. Addressing this issue requires the development of frameworks with more robust, irreversible bonds or strategies to protect susceptible sites. Scalability also presents a significant obstacle, since most PCOFs are synthesized via solvothermal methods that rely on elevated temperatures, high pressures, and large volumes of organic solvents, highlighting the need for more sustainable, low-temperature, or solvent-free synthetic approaches. Also, most PCOFs use the incorporation of a co-catalyst to suppress interfacial charge recombination during H_2 evolution. Platinum is predominantly used for this purpose, but its reliance as a noble metal significantly elevates the overall cost of hydrogen production [61]. Finally, achieving overall water splitting remains elusive because PCOFs generally exhibit limited water oxidation capabilities, necessitating the use of sacrificial agents for HER to retain only the reduction half reaction during hydrolysis, which leads to the waste of photogenerated vacancies [7].

4. Hybrid Porphyrinic Architectures

4.1. PMOF Heterojunctions

Heterojunction engineering based on porphyrinic MOFs (PMOFs) represents an effective strategy to overcome intrinsic limitations associated with charge recombination and restricted light utilization. By coupling PMOFs with narrow-band-gap semiconductors, favorable band alignments can be constructed that promote directional charge transfer and prolong charge-carrier lifetimes.

Wang et al. reported a series of Z-scheme heterojunctions, denoted as CuIn-PMOFs@$CdIn_2S_4$ (CuIn-PMOFs@CIS, 1–4), in which bimetallic Cu/In-PMOFs serve as crystalline templates to guide the layered growth of $CdIn_2S_4$ nanosheets via a solvothermal method. By varying the mass ratio of PMOFs to $CdIn_2S_4$ (2:10–5:10), the interfacial contact and charge-transfer efficiency were systematically tuned [60]. Among these composites, CuIn-PMOFs@CIS-3 exhibited the highest hydrogen evolution rate of 7.527 $mmol \cdot g^{-1} \cdot h^{-1}$, representing enhancements of 13.12-fold and 6.64-fold relative to pristine CIS and CuIn-PMOFs, respectively. This superior activity was attributed to synergistic integration of abundant metal active sites, broadened visible-light absorption, and efficient Z-scheme electron-transfer pathways from the conduction band of CIS to CuIn-, effectively suppressing charge recombination.

Similarly, embedding $ZnIn_2S_4$ (ZIS) nanosheets onto the Pd-PMOFs yielded Pd-PMOFs@ZIS heterojunctions with remarkably enhanced H_2 evolution rates of up to 8.2 $mmol \cdot g^{-1} \cdot h^{-1}$. This activity corresponds to increases of approximately 24.07-fold and 13.73-fold compared with pure ZIS and Pd-PMOFs, respectively. The improvement was ascribed to intimate interfacial assembly between the two components, facilitating rapid separation and migration of photoexcited charge carriers [50].

Another notable example of PMOF-based heterojunction engineering is the in situ growth of CdS nanoparticles within the porous channels of PCN-222(Pt), a Zr-based PMOF composed of TCPP porphyrin linkers containing atomically dispersed Pt sites. The resulting CdS@PCN-222(Pt) composite exhibited exceptionally high photocatalytic activity. When normalized to the mass of CdS, hydrogen evolution rates of approximately 71.6 $mmol \cdot g^{-1}$ (CdS)$\cdot h^{-1}$ under visible-light irradiation and 31.3 $mmol \cdot g^{-1}$ (CdS)$\cdot h^{-1}$ under sunlight were reported. This performance arises from uniform CdS dispersion within the high-surface-area MOF scaffold, ultrafast electron transfer to Pt single-atom sites anchored in the porphyrin cores, and the formation of intimate semiconductor-MOF heterojunctions that efficiently suppress charge recombination [74]).

Besides three-dimensional PMOFs, two-dimensional porphyrinic architectures also offer advantages for heterojunction construction. Xia et al. prepared a type-II heterojunction by growing CdS nanoparticles directly onto 2D Zn-TCPP nanosheets, forming CdS/Zn-TCPP nanocomposites (C–Z–T). In the presence of Pt as a cocatalyst, this composite achieved a hydrogen evolution rate of about 15.3 $mmol \cdot g^{-1} \cdot h^{-1}$ under visible-light irradiation. Notably, the C–Z–T system also exhibited activity in the near-infrared region, with measurable HER rates at 600, 765, and >800 nm, highlighting the potential of PMOF heterostructures for broadband solar utilization [75].

S-scheme heterojunctions provide another method to retain strong redox potential while suppressing recombination. Chen et al. combined solid-solution metal sulfide nanoparticles (ZCS-0.5) with metalated Zr-based PMOF-545M (M = Co, Ni, Cu, Zn) to construct ZCS/MOF-545M composites. Among these, ZCS-0.5/MOF-545Co exhibited the highest hydrogen evolution rate of 148 $mmol \cdot h^{-1}$, corresponding to enhancements of 52.8-, 22.9-, and 6.5-fold relative to ZnS, CdS, and ZCS-0.5 alone. The S-scheme configuration ensured effective spatial separation of charge carriers while preserving highly redox-active electrons and holes, thereby promoting efficient hydrogen evolution [76].

Alternative fabrication strategies have also been explored. Wu et al. constructed a CdS/Fe-MOF-525 composite via a facile ball-milling approach, introducing Fe atoms into the organic ligands of MOF-525. The optimized CdS/Fe-MOF-525-2.3 composite exhibited a hydrogen evolution rate of 3.6 $mmol \cdot g^{-1} \cdot h^{-1}$, outperforming the individual components. This enhancement was attributed to the formation of Fe-N_4 and Fe-N-C coordination motifs and the orderly interfacial assembly between CdS and the MOF matrix [77].

Furthermore, transition metal sulfides (TMSs), including Fe_xS_y, Co_xS_y, and Ni_xS_y, have been investigated as earth-abundant cocatalysts in PMOF heterojunctions [78]. Mi et al. deposited Ni_3S_4 and CoS_2 particles onto PCN-222(Zn), forming PCN-222(Zn)-Ni3S4 and PCN-222(Zn)-CoS_2 composites. In the presence of BIH as a sacrificial electron donor, PCN-222(Zn)-Ni_3S_4 exhibited the highest hydrogen evolution rate of 0.57 mmol $g^{-1}{\cdot}h^{-1}$, substantially exceeding that of PCN-222(Zn)-CoS_2 (0.155 mmol$\cdot g^{-1}\cdot h^{-1}$) and pristine PCN-222(Zn) (0.012 mmol$\cdot g^{-1}\cdot h^{-1}$). Photophysical studies confirmed that enhanced charge separation and interfacial electron migration in the Ni_3S_4-containing composite were responsible for its superior performance [79].

4.2. PCOF Heterojunctions

Constructing heterojunctions between PCOFs and inorganic semiconductors is a tool to enhance photocatalytic efficiency by aligning band structures and facilitating directional charge transfer. Guan et al. synthesized PCOF-18(Pt) by linking porphyrin units through robust C-C bonds while incorporating Pt atoms (19 wt%) with atomic-level dispersion. Subsequent integration of CdS yielded CdS@PCOF-18(Pt)-30, which displayed exceptional hydrogen evolution rates of 240.3 mmol$\cdot g^{-1}\cdot h^{-1}$ under full-spectrum irradiation and 110 mmol$\cdot g^{-1}\cdot h^{-1}$ under visible light ($\geq$420 nm). The remarkable activity was attributed to synergistic interactions between CdS and atomically dispersed Pt sites within the PCOF, enabling rapid charge transfer and efficient utilization of photogenerated carriers [80]. Additional heterostructures were prepared by growing TiO_2, ZnO, and $ZnIn_2S_4$ on PCOF-18(Pt), all of which exhibited significantly enhanced photocatalytic activity compared with the pristine framework. These results highlight the versatility of PCOF platforms for constructing multi-semiconductor heterojunctions with tailored interfacial properties.

A complementary approach involved constructing a 3D/2D type-II heterostructure by integrating $ZnIn_2S_4$ nanosheets with a Cu-TAPP-based COF, yielding $ZnIn_2S_4$@CuP–Ph COF (Figure 18). This composite achieved a hydrogen evolution rate of 2.67 mmol$\cdot g^{-1}\cdot h^{-1}$, attributed to synergistic enhancement of interfacial charge mobility and improved light-harvesting efficiency [81].

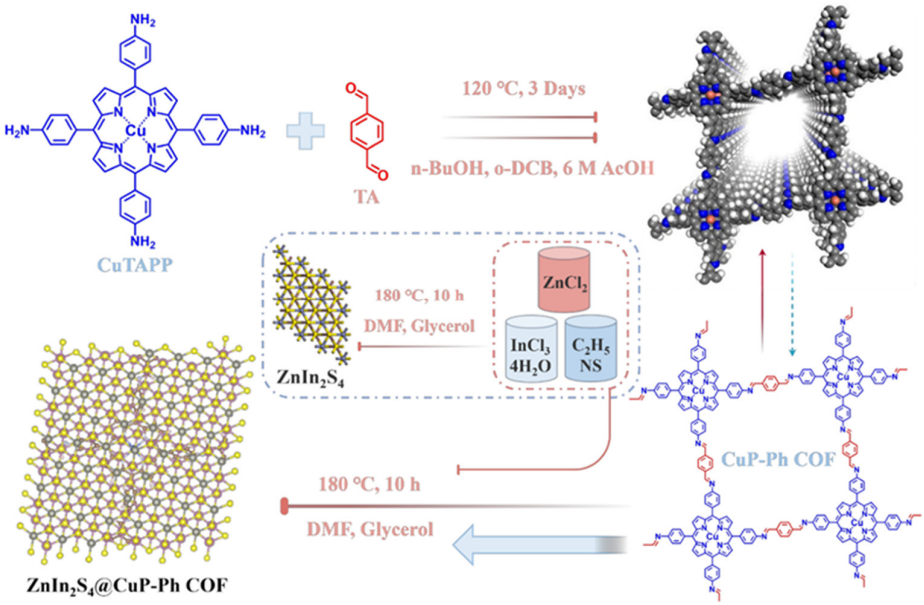


Figure 18. Synthesis of 3D/2D $ZnIn_2S_4$@CuP−Ph COF Heterojunction Photocatalyst. Reproduced from [81] with permission from American Chemical Society, License number 6176570226995.

Framework-level modification has also proven effective. Yao et al. incorporated Zn^{2+} ions and polyethylene glycol (PEG) into 2D TP-COFs, forming Zn-TP-COF@PEG (Figure 19).

The optimized material exhibited a hydrogen evolution rate of 0.186 mmol·g^{-1}·h^{-1}. The enhancement was attributed to Zn coordination within the porphyrin core, which facilitated photoexcited electron transport, together with PEG-induced refinement of the layered architecture and reinforcement of interlayer π–π interactions [71].

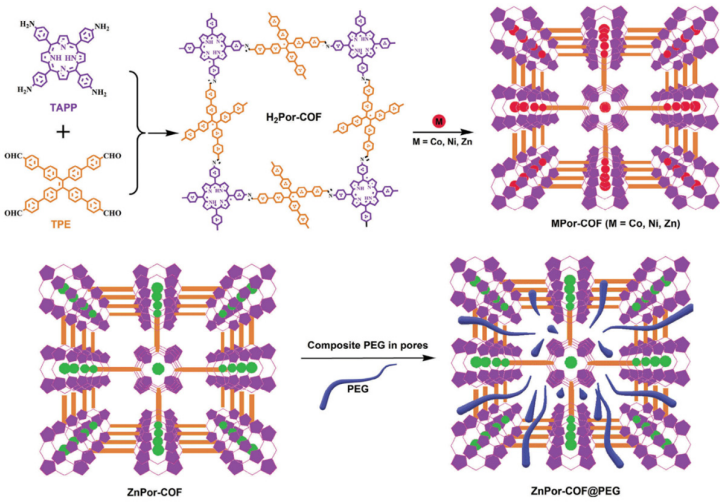


Figure 19. Synthesis of H_2Por-COF, MPor-COF (M = Co, Ni, Zn) and ZnPor-COF@PEG. Reproduced from [71] with permission from John Wiley and Sons, license number 6176570545431.

4.3. MOF/COF Heterojunctions

Hybrid architectures combining MOFs and COFs integrate the complementary advantages of both framework classes, offering high crystallinity, tunable porosity, and robust interfacial coupling. Ti-based MOFs are particularly attractive components due to their chemical stability and favorable electronic properties [82]. Using a covalent-integration strategy, Chen et al. developed a series of Ti-MOF/COF hybrid photocatalysts, denoted PdTCPP⊂PCN-415(NH_2)/TpPa, in which tetratopic Pd-metalated porphyrin ligands were incorporated into the Ti-MOF PCN-415(NH_2) and subsequently covalently linked to a TpPa COF (Figure 20). Among the resulting hybrids, the optimized composition (hybrid 2) exhibited the highest hydrogen evolution rate of 13.98 mmol·g^{-1}·h^{-1} and a turnover frequency of 227 h^{-1}, significantly outperforming the individual MOF and COF components. The enhanced activity was attributed to strong visible-light absorption, favorable band-gap alignment, high surface area, and improved structural robustness afforded by covalent coupling of the two frameworks [35].

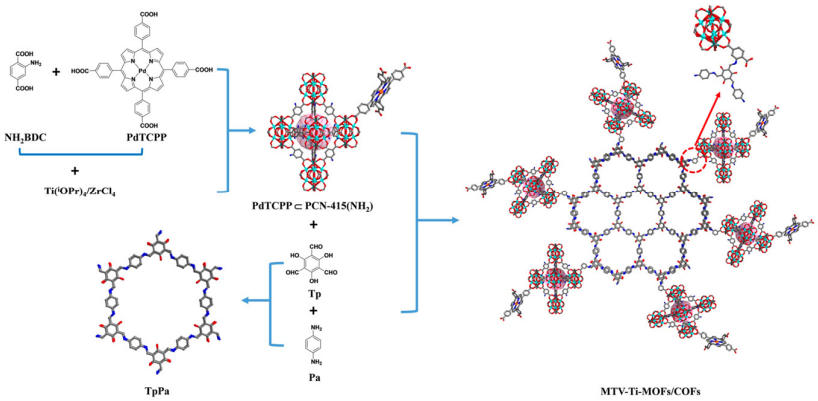


Figure 20. The schematic synthesis of MTV-Ti-MOF/COF. Reproduced from [35] with permission from John Wiley and Sons, license number 6176570715242.

5. Future Perspectives and Conclusions

In summary, photocatalytic water splitting based on PMOFs and PCOFs has gained significant attention as powerful platforms for photocatalytic water splitting and solar-to-chemical energy conversion. These materials combine abundant and tunable metal active sites with highly ordered crystalline architectures, permanent porosity, and large surface areas, enabling efficient visible-light harvesting and catalytic hydrogen evolution. While comparative studies performed under consistent experimental conditions provide valuable insight into the effects of porphyrin metalation, linker chemistry, and framework topology, the currently available data do not support definitive rankings of a universally "best" metal center or structural motif for photocatalytic H_2 evolution. Instead, performance is strongly context-dependent, governed by subtle interplays among electronic structure, morphology, charge-transfer pathways, and catalytic interfaces.

Looking forward, a central challenge lies in developing a deeper and more quantitative understanding of structure–activity relationships in PMOFs and PCOFs. Such insight is essential for the rational construction of multifunctional architectures that integrate optimal light harvesting, efficient charge separation, and rapid proton-reduction kinetics within a single framework. Achieving this level of control will require systematic tuning of both organic linkers and metal nodes to balance high catalytic efficiency with broad spectral response ideally extending into the near-infrared region while maintaining cost effectiveness. Promising directions include the incorporation of porphyrins bearing asymmetric substituents and the use of metal nodes with unconventional coordination environments, which offer additional degrees of freedom for modulating electronic structure and charge-transport behavior [57].

Equally critical is the improvement of structural robustness and long-term aqueous stability, which remains a major barrier to practical implementation. Many PMOFs and PCOFs exhibit excellent initial activity but suffer from gradual degradation under prolonged illumination or in water-rich environments. Addressing this issue will be essential before these materials can be considered for real-world applications [30]. In parallel, scalable and reproducible synthesis routes must be developed to enable the large-scale production of highly crystalline, porous frameworks without compromising performance. This challenge underscores the need for low-cost, rapid, and environmentally benign synthetic strategies that operate under mild conditions and avoid reliance on noble metals [9,62].

Finally, the integration of theoretical modeling, multiscale simulations, and machine-learning approaches is expected to play an increasingly important role in guiding future research. By correlating electronic structure, metal identity and concentration, framework topology, and catalytic performance, these tools can accelerate the discovery and optimization of porphyrin-based photocatalysts. In particular, such approaches hold promise for the rational design of materials tailored for challenging applications such as seawater splitting, where competing ion effects and complex interfacial phenomena must be carefully managed [21,83].

In conclusion, porphyrin-based framework materials represent a fertile and rapidly evolving platform for photocatalytic hydrogen production. Considerable opportunities remain for innovation in molecular design, structural engineering, and mechanistic understanding. Continued interdisciplinary efforts are expected to unlock new functionalities, further enhance performance, and ultimately expand the practical applicability of these systems in sustainable energy technologies.

Overall, these examples demonstrate that hybrid porphyrinic architecture provides a platform for overcoming intrinsic limitations of individual PMOFs or PCOFs, particularly with respect to charge recombination, light absorption, and catalytic kinetics. Rational selection of semiconductor partners, precise control of interfacial structure, and integration

of single-atom or low-loading cocatalysts are emerging as key design principles for next-generation hybrid photocatalysts.

Funding: This research received no external funding.

Institutional Review Board Statement: Not applicable.

Informed Consent Statement: Not applicable.

Data Availability Statement: No new data were created or analyzed in this study. Data sharing is not applicable to this article.

Acknowledgments: The authors take full responsibility for the content of this publication.

Conflicts of Interest: The authors declare no conflicts of interest.

Abbreviations

The following abbreviations are used in this manuscript:

CB	conduction band
COF	covalent organic frameworks
HER	hydrogen evolution reaction
HOMO	highest occupied molecular orbital
LCCT	ligand-to-cluster charge transfer
LMCT	ligand-to-metal charge-transfer
LUMO	lowest unoccupied molecular orbital
MOF	metal–organic frameworks
NIR	near-infrared
OER	oxygen evolution reaction
PCOFs	porphyrinic covalent organic frameworks
PMOFs	porphyrinic metal–organic frameworks
SBUs	secondary building units
UV	ultraviolet
VB	valence band

References

1. IEA. *Global Hydrogen Review 2023*; OECD Publishing: Paris, France, 2023. [CrossRef]
2. Terlouw, T.; Rosa, L.; Bauer, C.; McKenna, R. Future Hydrogen Economies Imply Environmental Trade-Offs and a Supply-Demand Mismatch. *Nat. Commun.* **2024**, *15*, 7043. [CrossRef] [PubMed]
3. Hisatomi, T.; Domen, K. Reaction Systems for Solar Hydrogen Production via Water Splitting with Particulate Semiconductor Photocatalysts. *Nat. Catal.* **2019**, *2*, 387–399. [CrossRef]
4. Pourasl, H.H.; Barenji, R.V.; Khojastehnezhad, V.M. Solar Energy Status in the World: A Comprehensive Review. *Energy Rep.* **2023**, *10*, 3474–3493. [CrossRef]
5. Tashie-Lewis, B.C.; Nnabuife, S.G. Hydrogen Production, Distribution, Storage and Power Conversion in a Hydrogen Economy—A Technology Review. *Chem. Eng. J. Adv.* **2021**, *8*, 100172. [CrossRef]
6. Dang, V.-H.; Nguyen, T.-A.; Le, M.-V.; Nguyen, D.Q.; Wang, Y.H.; Wu, J.C.-S. Photocatalytic Hydrogen Production from Seawater Splitting: Current Status, Challenges, Strategies and Prospective Applications. *Chem. Eng. J.* **2024**, *484*, 149213. [CrossRef]
7. Zhu, S.-S.; Zhang, Z.; Li, Z.; Liu, X. Recent Progress on Covalent Organic Frameworks for Photocatalytic Hydrogen Generation via Water Splitting. *Mater. Chem. Front.* **2024**, *8*, 1513–1535. [CrossRef]
8. Tian, L.; Guan, X.; Zong, S.; Dai, A.; Qu, J. Cocatalysts for Photocatalytic Overall Water Splitting: A Mini Review. *Catalysts* **2023**, *13*, 355. [CrossRef]
9. Prakash, K.; Mishra, B.; Díaz, D.D.; Nagaraja, C.M.; Pachfule, P. Strategic Design of Covalent Organic Frameworks (COFs) for Photocatalytic Hydrogen Generation. *J. Mater. Chem. A* **2023**, *11*, 14489–14538. [CrossRef]
10. Chen, X.; Shen, S.; Guo, L.; Mao, S.S. Semiconductor-Based Photocatalytic Hydrogen Generation. *Chem. Rev.* **2010**, *110*, 6503–6570. [CrossRef]
11. Kheradmand, A.; Zhu, Y.; Gu, S.; Jiang, Y. Photocatalytic Hydrogen Evolution. In *Solar-to-Chemical Conversion*; Sun, H., Ed.; Wiley-VCH: Weinheim, Germany, 2021; pp. 77–105.

12. You, J.; Zhao, Y.; Wang, L.; Bao, W. Recent Developments in the Photocatalytic Applications of Covalent Organic Frameworks: A Review. *J. Clean. Prod.* **2021**, *291*, 125822. [CrossRef]
13. Ladomenou, K.; Natali, M.; Iengo, E.; Charalampidis, G.; Scandola, F.; Coutsolelos, A.G. Photochemical Hydrogen Generation with Porphyrin-Based Systems. *Coord. Chem. Rev.* **2015**, *304–305*, 38–54. [CrossRef]
14. Panagiotopoulos, A.; Ladomenou, K.; Sun, D.; Artero, V.; Coutsolelos, A.G. Photochemical Hydrogen Production and Cobaloximes: The Influence of the Cobalt Axial N-Ligand on the System Stability. *Dalton Trans.* **2016**, *45*, 6732–6738. [CrossRef] [PubMed]
15. Nikoloudakis, E.; Coutsolelos, A.G.; Stratakis, E. Mini-Review on Catalytic Hydrogen Evolution from Porphyrin–Graphene Structures. *Energy Fuels* **2024**, *38*, 19222–19235. [CrossRef] [PubMed]
16. Landrou, G.; Panagiotopoulos, A.A.; Ladomenou, K.; Coutsolelos, A.G. Photochemical Hydrogen Evolution Using Sn-Porphyrin as Photosensitizer and a Series of Cobaloximes as Catalysts. *J. Porphyr. Phthalocyanines* **2016**, *20*, 534–541. [CrossRef]
17. Xu, F.; Weng, B. Photocatalytic Hydrogen Production: An Overview of New Advances in Structural Tuning Strategies. *J. Mater. Chem. A* **2023**, *11*, 4473–4486. [CrossRef]
18. Nikolaou, V.; Agapaki, E.; Nikoloudakis, E.; Achilleos, K.; Ladomenou, K.; Charalambidis, G.; Triantafyllou, E.; Coutsolelos, A.G. Highly Efficient Light-Driven Hydrogen Evolution Utilizing Porphyrin-Based Nanoparticles. *Chem. Commun.* **2023**, *59*, 11256–11259. [CrossRef]
19. Nikolaou, V.; Charalambidis, G.; Ladomenou, K.; Nikoloudakis, E.; Drivas, C.; Vamvasakis, I.; Panagiotakis, S.; Landrou, G.; Agapaki, E.; Stangel, C.; et al. Controlling Solar Hydrogen Production by Organizing Porphyrins. *ChemSusChem* **2021**, *14*, 961–970. [CrossRef]
20. Charisiadis, A.; Nikolaou, V.; Nikoloudakis, E.; Ladomenou, K.; Charalambidis, G.; Coutsolelos, A.G. Metalloporphyrins in Bio-Inspired Photocatalytic Conversions. *Chem. Commun.* **2025**, *61*, 4630–4646. [CrossRef]
21. Li, R.; Luan, J.; Zhang, Y.; Jiang, L.; Yan, H.; Chi, Q.; Yan, Z. A Review of Efficient Photocatalytic Water Splitting for Hydrogen Production. *Renew. Sustain. Energy Rev.* **2024**, *206*, 114863. [CrossRef]
22. Islam, A.; Malek, A.; Islam, M.T.; Nipa, F.Y.; Raihan, O.; Mahmud, H.; Uddin, M.E.; Ibrahim, M.L.; Abdulkareem-Alsultan, G.; Mondal, A.H.; et al. Next Frontier in Photocatalytic Hydrogen Production through CdS Heterojunctions. *Int. J. Hydrogen Energy* **2025**, *101*, 173–211. [CrossRef]
23. Bitsos, D.R.; Salepis, A.; Orfanos, E.; Coutsolelos, A.G.; Kosheleva, R.I.; Mitropoulos, A.C.; Ladomenou, K. Exploring Metal- and Porphyrin-Modified TiO_2-Based Photocatalysts for Efficient and Sustainable Hydrogen Production. *Inorganics* **2025**, *13*, 121. [CrossRef]
24. Yan, Y.; Meng, Q.; Tian, L.; Cai, Y.; Zhang, Y.; Chen, Y. Engineering of *g*-C_3N_4 for Photocatalytic Hydrogen Production: A Review. *Int. J. Mol. Sci.* **2024**, *25*, 8842. [CrossRef]
25. Tang, C.; Li, X.; Hu, Y.; Du, X.; Wang, S.; Chen, B.; Wang, S. Porphyrin-Based Metal-Organic Framework Materials: Design, Construction, and Application in the Field of Photocatalysis. *Molecules* **2024**, *29*, 467. [CrossRef]
26. Asselin, P.; Harvey, P.D. Visible-Light-Driven Production of Solar Fuels Catalyzed by Nanosized Porphyrin-Based Metal–Organic Frameworks and Covalent–Organic Frameworks: A Review. *ACS Appl. Nano Mater.* **2022**, *5*, 6055–6082. [CrossRef]
27. Harvey, P.D. Porphyrin-Based Metal- and Covalent-Organic Frameworks as Heterogeneous Nanosized Photocatalysts in Organic Synthesis. *J. Mater. Chem. C* **2021**, *9*, 16885–16910. [CrossRef]
28. Zhang, X.; Liu, Z.; Shao, B.; Liang, Q.; Wu, T.; Pan, Y.; He, Q.; He, M.; Ge, L.; Huang, J. Porphyrin-Based Metal-Organic Framework Photocatalysts: Structure, Mechanism and Applications. *Small Methods* **2025**, *9*, 2402096. [CrossRef]
29. Li, Z.; Liu, C.; Deng, Q.; Deng, W. Rational Design of Covalent Organic Frameworks as Photocatalysts for Water Splitting. *Adv. Funct. Mater.* **2024**, *34*, 2402676. [CrossRef]
30. Rana, G.; Dhiman, P.; Kumar, A.; Wang, T.; Sharma, G. Recent Advances in Porphyrin-Based Metal Organic Frameworks and Composites for Photocatalytic Hydrogen Evolution and Water Treatment. *Chem. Eng. Res. Des.* **2023**, *199*, 620–638. [CrossRef]
31. Liu, R.; Jia, Y.; Xia, Y.; Wang, S. Metalloporphyrin-Based Covalent Organic Frameworks: Design, Construction, and Photocatalytic Applications. *Catalysts* **2026**, *16*, 76. [CrossRef]
32. Liu, F.; Rincón, I.; Baldoví, H.G.; Dhakshinamoorthy, A.; Horcajada, P.; Rojas, S.; Navalón, S.; Fateeva, A. Porphyrin-Based MOFs for Photocatalysis in Water: Advancements in Solar Fuels Generation and Pollutants Degradation. *Inorg. Chem. Front.* **2024**, *11*, 2212–2245. [CrossRef]
33. Lin, C.; Han, C.; Zhang, H.; Gong, L.; Gao, Y.; Wang, H.; Bian, Y.; Li, R.; Jiang, J. Porphyrin-Based Metal–Organic Frameworks for Efficient Photocatalytic H_2 Production under Visible-Light Irradiation. *Inorg. Chem.* **2021**, *60*, 3988–3995. [CrossRef]
34. Ha, J.; Lee, J.H.; Moon, H.R. Alterations to Secondary Building Units of Metal–Organic Frameworks for the Development of New Functions. *Inorg. Chem. Front.* **2020**, *7*, 12–27. [CrossRef]
35. Chen, C.; Xiong, Y.; Zhong, X.; Lan, P.C.; Wei, Z.; Pan, H.; Su, P.; Song, Y.; Chen, Y.; Nafady, A.; et al. Enhancing Photocatalytic Hydrogen Production via the Construction of Robust Multivariate Ti-MOF/COF Composites. *Angew. Chem. Int. Ed.* **2022**, *61*, e202114071. [CrossRef]

36. Pan, Y.; Abazari, R.; Tahir, B.; Sanati, S.; Zheng, Y.; Tahir, M.; Gao, J. Iron-Based Metal–Organic Frameworks and Their Derived Materials for Photocatalytic and Photoelectrocatalytic Reactions. *Coord. Chem. Rev.* **2024**, *499*, 215538. [CrossRef]
37. Yan, F.; Zhang, Y.; Liu, S.; Zou, R.; Ghasemi, J.B.; Li, X. Efficient Charge Separation by a Donor-Acceptor System Integrating Dibenzothiophene into a Porphyrin-Based Metal-Organic Framework for Enhanced Photocatalytic Hydrogen Evolution. *Chin. J. Catal.* **2023**, *51*, 124–134. [CrossRef]
38. Fu, R.; Wang, L.; Wang, K.; Li, C.; Ouyang, M.; Zhang, C.; Wu, H.; Zhang, Q. Titanium-Based Metal-Organic Frameworks: Synthesis Innovations and Multifunctional Applications. *Coord. Chem. Rev.* **2025**, *541*, 216832. [CrossRef]
39. Yang, G.; Lv, J.; Yang, Q.; Wang, Q. Full-Spectrum Photocatalytic Hydrogen Production by MOFs Materials-A Minireview. *Mater. Today Sustain.* **2025**, *31*, 101186. [CrossRef]
40. Xu, J.; Li, Z.; Wang, R.; Zhang, X.; Zhang, X.; Wei, Y.; Hou, X.; Liu, Y. Metalloporphyrin-Sensitized Ti Metal–Organic Framework Nanostructures for Visible-Light-Driven Hydrogen Evolution. *ACS Appl. Nano Mater.* **2025**, *8*, 2179–2187. [CrossRef]
41. Feng, H.; Li, H.; Liu, X.; Huang, Y.; Pan, Q.; Peng, R.; Du, R.; Zheng, X.; Yin, Z.; Li, S.; et al. Porphyrin-Based Ti-MOFs Conferred with Single-Atom Pt for Enhanced Photocatalytic Hydrogen Evolution and NO Removal. *Chem. Eng. J.* **2022**, *428*, 132045. [CrossRef]
42. Koschnick, C.; Stäglich, R.; Scholz, T.; Terban, M.W.; Von Mankowski, A.; Savasci, G.; Binder, F.; Schökel, A.; Etter, M.; Nuss, J.; et al. Understanding Disorder and Linker Deficiency in Porphyrinic Zirconium-Based Metal–Organic Frameworks by Resolving the Zr_8O_6 Cluster Conundrum in PCN-221. *Nat. Commun.* **2021**, *12*, 3099. [CrossRef]
43. Mandal, S.; Leiter, R.; Biskupek, J.; Kaiser, U.; Pannwitz, A. The Zr_8O_6 Secondary Building Unit and Porphyrin Linker Catalyze Light-Driven H_2 Evolution in Porphyrin-Based Metal Organic Frameworks. *ChemSusChem* **2025**, *18*, e202500372. [CrossRef] [PubMed]
44. Kim, J.H.; Wu, S.; Zdrazil, L.; Denisov, N.; Schmuki, P. 2D Metal–Organic Framework Nanosheets Based on Pd-TCPP as Photocatalysts for Highly Improved Hydrogen Evolution. *Angew. Chem. Int. Ed.* **2024**, *63*, e202319255. [CrossRef] [PubMed]
45. Chen, M.; Zhang, C.; Tang, Y.; Cai, Q.; Yu, J.; Chen, Y.; He, Y.; Bai, J.; Fu, M.; Chen, S. Cu Ions Anchored in the Porphyrin Center Act as Transient Metal Centers of 2D-MOFs to Enhance Photocatalytic Hydrogen Production. *Catal. Sci. Technol.* **2023**, *13*, 581–586. [CrossRef]
46. Li, H.; Liu, X.; He, Y.; Feng, H.; Zhang, Y.; Liu, C.; Wu, Z. 2D Porphyrin-Based MOFs with Highly Dispersed Pt Nanoparticles via in-Situ Partial Reduction Strategy from Porphyrin Embedded with Single-Atom Pt for Enhancing Photocatalytic Hydrogen Production. *Fuel* **2023**, *338*, 127369. [CrossRef]
47. Wang, X.; Zhang, X.; Zhou, W.; Liu, L.; Ye, J.; Wang, D. An Ultrathin Porphyrin-Based Metal-Organic Framework for Efficient Photocatalytic Hydrogen Evolution under Visible Light. *Nano Energy* **2019**, *62*, 250–258. [CrossRef]
48. Mo, Q.; Zhang, L.; Li, S.; Song, H.; Fan, Y.; Su, C.-Y. Engineering Single-Atom Sites into Pore-Confined Nanospaces of Porphyrinic Metal–Organic Frameworks for the Highly Efficient Photocatalytic Hydrogen Evolution Reaction. *J. Am. Chem. Soc.* **2022**, *144*, 22747–22758. [CrossRef]
49. Xiao, L.; Zhang, Q.; Wang, X.; Li, B.; Li, X.; Yang, X.; Li, W.; Zhang, H. Integration of Platinum Nanoparticles and Pd-Porphyrin Photosensitiser into a Metal–Organic Framework for Effective Photocatalytic Hydrogen Evolution. *J. Colloid Interface Sci.* **2025**, *685*, 165–172. [CrossRef]
50. Wang, S.; Feng, H.; Zheng, C.; Li, S.; Fan, S.; Feng, Y.-S. Fabrication of Heterostructured Pd-Porphyrin MOFs/$ZnIn_2S_4$ Composites to Boost Photocatalytic Hydrogen Evolution Under Visible Light Irradiation. *Inorg. Chem. Front.* **2023**, *10*, 4471–4483. [CrossRef]
51. Leng, F.; Liu, H.; Ding, M.; Lin, Q.-P.; Jiang, H.-L. Boosting Photocatalytic Hydrogen Production of Porphyrinic MOFs: The Metal Location in Metalloporphyrin Matters. *ACS Catal.* **2018**, *8*, 4583–4590. [CrossRef]
52. Navalón, S.; Dhakshinamoorthy, A.; Álvaro, M.; Ferrer, B.; García, H. Metal–Organic Frameworks as Photocatalysts for Solar-Driven Overall Water Splitting. *Chem. Rev.* **2023**, *123*, 445–490. [CrossRef]
53. Wang, S.; Li, S.; Zheng, C.; Feng, H.; Feng, Y.-S. Bimetallic Porphyrin-Based Metal–Organic Framework as a Superior Photocatalyst for Enhanced Photocatalytic Hydrogen Production. *Inorg. Chem.* **2024**, *63*, 554–563. [CrossRef]
54. Banerjee, T.; Gottschling, K.; Savasci, G.; Ochsenfeld, C.; Lotsch, B.V. H_2 Evolution with Covalent Organic Framework Photocatalysts. *ACS Energy Lett.* **2018**, *3*, 400–409. [CrossRef]
55. Mohamadpour, F.; Amani, A.M. Photocatalytic Systems: Reactions, Mechanism, and Applications. *RSC Adv.* **2024**, *14*, 20609–20645. [CrossRef] [PubMed]
56. Prieto, T.; Ponte, C.; Guntermann, R.; Medina, D.D.; Salonen, L.M. Synthetic Strategies to Extended Aromatic Covalent Organic Frameworks. *Chem. Eur. J.* **2024**, *30*, e202401344. [CrossRef] [PubMed]
57. Gu, J.; Peng, Y.; Zhou, T.; Ma, J.; Pang, H.; Yamauchi, Y. Porphyrin-Based Framework Materials for Energy Conversion. *Nano Res. Energy* **2022**, *1*, e9120009. [CrossRef]
58. Song, Y.-X.; Wang, Z.; Zhang, Y.-H. Enhancing Charge Transfer Efficiency through Carboxyl-Modification to Improve the Photocatalytic Activity of Covalent Organic Frameworks for Hydrogen Evolution from Water Splitting. *J. Colloid Interface Sci.* **2025**, *686*, 348–358. [CrossRef]

59. Chen, M.; Li, H.; Liu, C.; Liu, J.; Feng, Y.; Wee, A.G.H.; Zhang, B. Porphyrin- and Porphyrinoid-Based Covalent Organic Frameworks (COFs): From Design, Synthesis to Applications. *Coord. Chem. Rev.* **2021**, *435*, 213778. [CrossRef]
60. Wang, S.; Hu, G.; Dou, Y.; Li, S.; Li, M.; Feng, H.; Feng, Y.-S. Z-Scheme Promoted Interfacial Charge Transfer on Cu/In-Porphyrin MOFs/$CdIn_2S_4$ Heterostructure for Efficient Photocatalytic H_2 Evolution. *Sep. Purif. Technol.* **2025**, *354*, 129220. [CrossRef]
61. Chen, M.; Fu, G.; Zhao, W.; Zhang, T. Effective Strategies in Covalent Organic Frameworks for Enhanced Photocatalytic Hydrogen Production. *Chem. Eur. J.* **2025**, *31*, e202500100. [CrossRef]
62. Gu, C.-C.; Xu, F.-H.; Zhu, W.-K.; Wu, R.-J.; Deng, L.; Zou, J.; Weng, B.-C.; Zhu, R.-L. Recent Advances on Covalent Organic Frameworks (COFs) as Photocatalysts: Different Strategies for Enhancing Hydrogen Generation. *Chem. Commun.* **2023**, *59*, 7302–7320. [CrossRef]
63. Liu, S.; Wang, M.; Wang, S.; Hu, H.; Sun, J.; Wang, J.; Su, X.; Lu, H.; Gao, Y. Construction of Porphyrin-Based Two-Dimensional Covalent Organic Frameworks for Photocatalytic Hydrogen Production. *Catal. Sci. Technol.* **2024**, *14*, 4236–4244. [CrossRef]
64. He, T.; Zhen, W.; Chen, Y.; Guo, Y.; Li, Z.; Huang, N.; Li, Z.; Liu, R.; Liu, Y.; Lian, X.; et al. Integrated Interfacial Design of Covalent Organic Framework Photocatalysts to Promote Hydrogen Evolution from Water. *Nat. Commun.* **2023**, *14*, 329. [CrossRef] [PubMed]
65. Yang, Y.; Peng, S.; Chen, S.; Kang, F.; Fan, J.; Zhang, H.; Yu, X.; Li, J.; Zhang, Q. Pyrene-Based Covalent Organic Frameworks (PyCOFs): A Review. *Nanoscale Horiz.* **2024**, *9*, 2198–2233. [CrossRef] [PubMed]
66. Huan, Z.; Bing, H.; Changyu, Q.; Xuxin, F.; Yiyong, H.; Xianglin, Y.; Junbo, L. Construction of Porphyrin-Pyrimidine 1D Covalent Organic Framework (1D-COF) with Dual Photocatalytic Hydrogen and Oxygen Evolution. *J. Solid State Chem.* **2026**, *354*, 125736. [CrossRef]
67. Chen, R.; Wang, Y.; Ma, Y.; Mal, A.; Gao, X.-Y.; Gao, L.; Qiao, L.; Li, X.-B.; Wu, L.-Z.; Wang, C. Rational Design of Isostructural 2D Porphyrin-Based Covalent Organic Frameworks for Tunable Photocatalytic Hydrogen Evolution. *Nat. Commun.* **2021**, *12*, 1354. [CrossRef]
68. Xu, Z.; Cui, X.; Li, Y.; Li, Y.; Si, Z.; Duan, Q. Tetraphenylethylene and Porphyrin-Based Covalent Organic Framework with Square Lattice for Effective Photocatalytic Hydrogen Evolution. *Appl. Surf. Sci.* **2023**, *613*, 155966. [CrossRef]
69. Lv, M.; Ren, X.; Cao, R.; Chang, Z.; Chang, X.; Bai, F.; Li, Y. Zn (II) Porphyrin Built-in D–A Covalent Organic Framework for Efficient Photocatalytic H_2 Evolution. *Polymers* **2022**, *14*, 4893. [CrossRef]
70. Lu, M.; Zhang, S.; Yang, M.; Liu, Y.; Liao, J.; Huang, P.; Zhang, M.; Li, S.; Su, Z.; Lan, Y. Dual Photosensitizer Coupled Three-Dimensional Metal-Covalent Organic Frameworks for Efficient Photocatalytic Reactions. *Angew. Chem.* **2023**, *135*, e202307632. [CrossRef]
71. Yao, C.; Wang, S.; Zha, Y.; Xu, Y. 2D Porphyrin-Based Covalent–Organic Framework/PEG Composites: A Rational Strategy for Photocatalytic Hydrogen Evolution. *Macromol. Rapid Commun.* **2024**, *45*, 2400250. [CrossRef]
72. Han, Y.; Jin, Y.; Yang, G.; Ma, X.; Wang, X.; Qi, D.; Wang, T.; Jiang, J. Covalent Organic Framework Controls the Aggregation of Metal Porphyrins for Enhanced Photocatalytic H_2 Evolution. *Chem. Asian J.* **2025**, *20*, e202401342. [CrossRef]
73. Khan, N.; Azad, C.; Luo, M.; Chen, J.; Kesharwani, T.; Badshah, A.; Wang, D. Mechanistic Approach towards Designing Covalent Organic Frameworks for Photocatalytic Hydrogen Generation. *Energies* **2023**, *16*, 5888. [CrossRef]
74. Guan, G.-W.; Zheng, S.-T.; Xia, M.; Li, K.-X.; Ouyang, Y.-S.; Yang, G.; Yang, Q.-Y. Incorporating CdS and Anchoring Pt Single Atoms into Porphyrinic Metal–Organic Frameworks for Superior Visible-Light and Sunlight-Driven H_2 Evolution. *Chem. Eng. J.* **2023**, *464*, 142530. [CrossRef]
75. Xia, Z.; Yu, R.; Yang, H.; Luo, B.; Huang, Y.; Li, D.; Shi, J.; Xu, D. Novel 2D Zn-Porphyrin Metal Organic Frameworks Revived CdS for Photocatalysis of Hydrogen Production. *Int. J. Hydrogen Energy* **2022**, *47*, 13340–13350. [CrossRef]
76. Chen, M.; Umer, K.; Li, B.; Li, Z.; Li, K.; Sun, W.; Ding, Y. Metalloporphyrin Based MOF-545 Coupled with Solid Solution ZnxCd1-xS for Efficient Photocatalytic Hydrogen Production. *J. Colloid Interface Sci.* **2024**, *653*, 380–389. [CrossRef] [PubMed]
77. Wu, Y.; Qu, Y.; Su, C.; Yang, X.; Yang, Y.; Zhang, Y.; Huang, W. Enhanced Photoinduced Carrier Separation in Fe-MOF-525/CdS for Photocatalytic Hydrogen Evolution: Improved Catalytic Dynamics with Specific Active Sites. *Inorg. Chem.* **2023**, *62*, 21290–21298. [CrossRef] [PubMed]
78. Ding, Y.; Gao, Z.; Xiang, H. Synthesis and Structural Engineering of Transition Metal Sulfides: Advances in Improving Hydrogen Evolution Reaction Catalytic Efficiency. *Inorganics* **2025**, *13*, 84. [CrossRef]
79. Mi, F.; Fang, Z.; Li, J.; Yang, C.; Zhang, T. Porphyrinic Metal-Organic Framework-Based Heterojunction Composites for Enhanced Photocatalytic Hydrogen Evolution. *Adv. Funct. Mater.* **2025**, *35*, 2506838. [CrossRef]
80. Guan, G.-W.; Zheng, S.-T.; Zhang, L.-P.; Hou, S.-Y.; Liu, X.-Y.; Yang, Q.-Y. Incorporating Atomic-Level Center into Porphyrin-Based COF for Photocatalytic H_2 Evolution. *Chem. Eng. J.* **2025**, *514*, 163127. [CrossRef]
81. Xia, Y.; Huang, G.; Fan, Y.; Zhao, X.; Wang, L.; Huang, J.; She, H.; Wang, Q. Preparation of 3D/2D $ZnIn_2S_4$/Porphyrin (Cu)-COF Type II Heterojunction: An In-Depth Insight into Interfacial Charge Transfer for Efficient Light-to-Hydrogen Conversion. *J. Phys. Chem. C* **2024**, *128*, 15000–15011. [CrossRef]

82. Altintas, C.; Erucar, I.; Keskin, S. MOF/COF Hybrids as next Generation Materials for Energy and Biomedical Applications. *CrystEngComm* **2022**, *24*, 7360–7371. [CrossRef]
83. Niu, H.; Zhu, G.; Zhang, S.; Wang, T.; Wang, Q.; Yang, X.; Li, X.; Zhu, F.; Wu, G.; Yu, H. Porphyrin-Based Heterojunction Photocatalysts: Design Principles and Applications in Solar-to-Chemical Energy Conversion. *J. Mater. Chem. A* **2025**, *13*, 32030–32055. [CrossRef]

Disclaimer/Publisher's Note: The statements, opinions and data contained in all publications are solely those of the individual author(s) and contributor(s) and not of MDPI and/or the editor(s). MDPI and/or the editor(s) disclaim responsibility for any injury to people or property resulting from any ideas, methods, instructions or products referred to in the content.